AD-A063 387 JAYCOR ALEXANDRIA VA F/G 9/5
STUDY ON THE INITIAL DEVELOPMENT OF HIGH-POWER MILLIMETER WAVE --ETC(U)
1979 M READ, R LUCEY N00173-77-C-0215
UNCLASSIFIED NL

1 OF 1
AD A063387

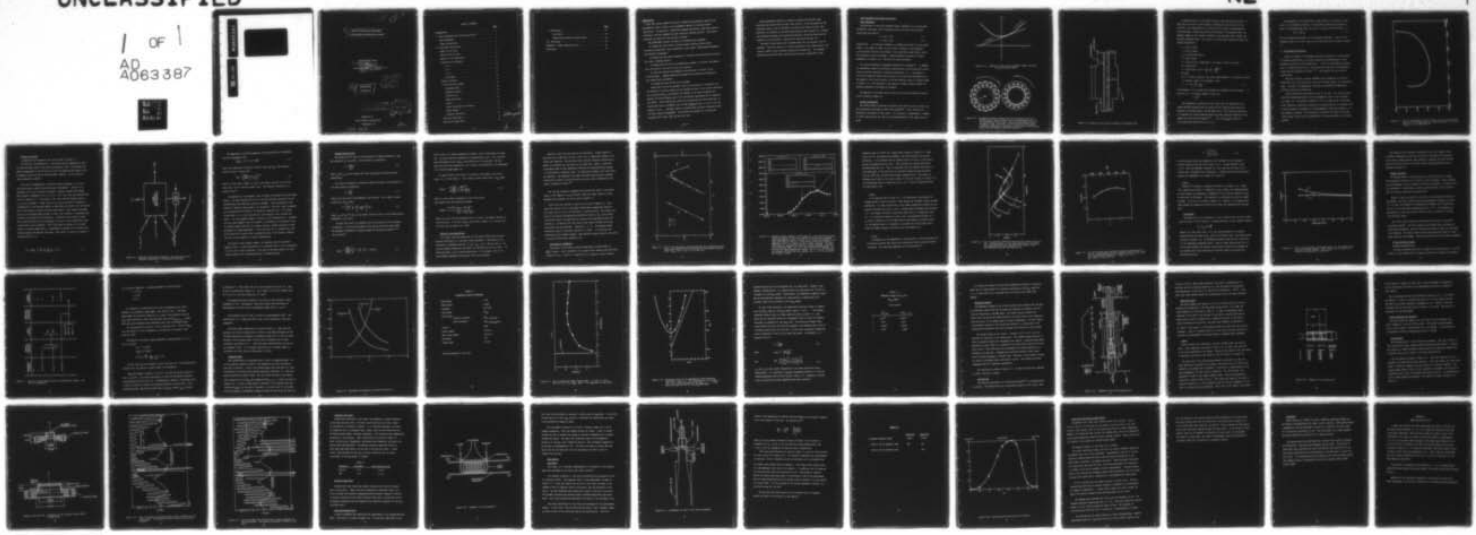

END
DATE FILMED
3-79
DDC

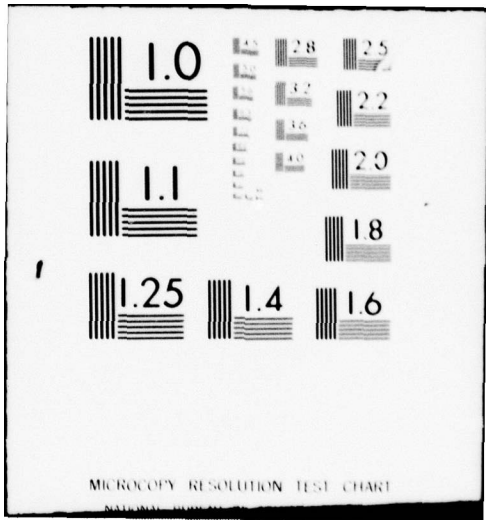
1.0
1.1
1.25
1.4
1.6
2.8
2.5
2.2
2.0
1.8
MICROCOPY RESOLUTION TEST CHART

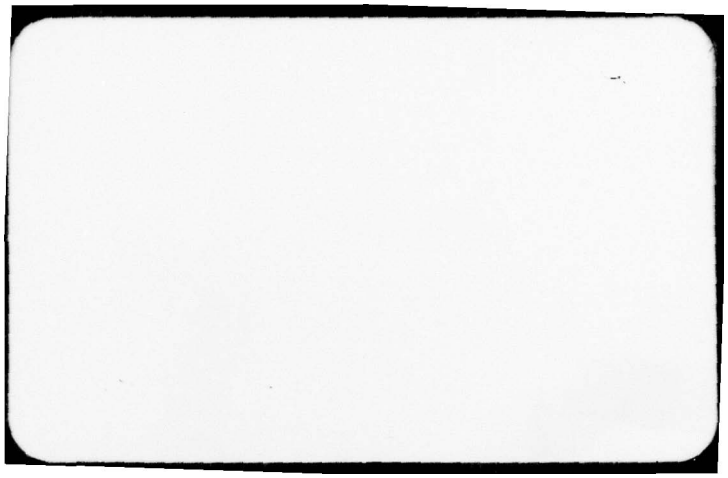

LEVEL II (1) 82

(6) STUDY ON THE INITIAL DEVELOPMENT OF HIGH-POWER MILLIMETER WAVE SOURCES.

JAYCOR PROJECT #2061

(9) Final Report on NRL

Contract No. (15) N00173-77-C-0215 Rev

(11) 1979

(12) 56p.

(10) Michael Read

Robert Lucey

Submitted to

Naval Research Laboratories

Washington, DC

Gen

393 453

TABLE OF CONTENTS

INTRODUCTION

Under NRL contract #N00173-77-C-0215, JAYCOR has performed an analytic and experimental study of some of the fundamental aspects of cyclotron masers (gyrotrons). In particular, JAYCOR has designed and tested a high power gyrotron oscillator, and has designed and used a gyrotron testing facility. This report discusses the results of this project in detail.

The JAYCOR-NRL contract includes the following work statement:

(1) Design and test a 200 kw cyclotron maser testing facility which includes the modulator, pulse transformer, power supply, superconducting magnet, and auxiliary subsystems.

(2) Design and test maser components to include the RF interaction structure and output coupling network.

(3) Design and test the RF instrumentation package to include a millimeter wave calorimetric load and an output mode analyzer.

(4) Test and evaluate the magnetron injection gun to be used in the cyclotron maser. Compare measured performance with theoretical predictions and optimize gun performance.

(5) Design and test the RF driver package.

Essentially this work statement calls for the design of a laboratory for the testing of cyclotron masers and the design and test of the various components of an initial device. One element not defined in the above statement was whether the initial device was to be an oscillator (gyronmonotron) or amplifier (gyro-TWA). After some initial study and consultation with NRL scientists, it was decided that an oscillator was the best <u>initial</u> device, in that it was the simpler of the two, and most likely to quickly yield the most information about the basic physical mechanisms. No RF driver was needed for an oscillator, therefore this report will not deal with one.

While preliminary plans for a system to analyze the electron beam characteristics were drawn up under this contract, it was determined by NRL scientists that it was not feasible to construct the device at that time. Therefore, no analysis on the beam characteristics was carried out. Instead, more extensive testing of the gyrotron system as a whole was done than was called for in the contract. This work is reported in Section III.

The body of this report will be broken down into two sections, and an appendix. The first section is a short discussion of the linear theory, the second a report on the nonlinear analysis and design work. The appendix describes the gyrotron test facility which has been established at NRL.

I. Basic Mechanism and Linear Calculation

Basic Mechanism

The gyrotron, or cyclotron resonance maser, mechanism, is a relativistic instability involving a fast waveguide mode and the fast cyclotron mode. These modes are given by

$$\omega^2 = k^2c^2 + \omega_{co}^2 \qquad 1.1$$

$$\omega = kv_{\parallel} + \Omega_c/\gamma \qquad 1.2$$

respectively. ω is the wave frequency, in radians per second, k is the wavenumber, c the speed of light, ω_{co} the cutoff frequency of the waveguide, $v_{\parallel}$ the parallel velocity of the beam, γ the relativistic mass factor, and Ω_c the classical cyclotron frequency. These dispersion relations are shown graphically in Figure 1.1a. The modes are shown uncoupled.

The actual mechanism is discussed extensively by Sprangle[1]. In summary, the instability results from electron bunching that occurs because the relativistic cyclotron frequency is inversely proportional to γ. The energy to drive the instability comes from the motion of the electrons perpendicular to the magnetic field, which couples to the wave electric field in a manner shown in Figure 1.1b. The electrons in the figure are shown already bunched--the bunching mechanism is discussed by Sprangle.

The geometry of the model used for both the linear and nonlinear calculations is shown in Figure 1.2.

Linear Calculations

The linear theory of gyrotron oscillators with right circular cavities has been extensively developed by Chu[2] and Sprangle[1]. Chu's work will be extensively referenced in this report. For the sake of completeness, a summary of their results which are used in the design methods of this report will be given.

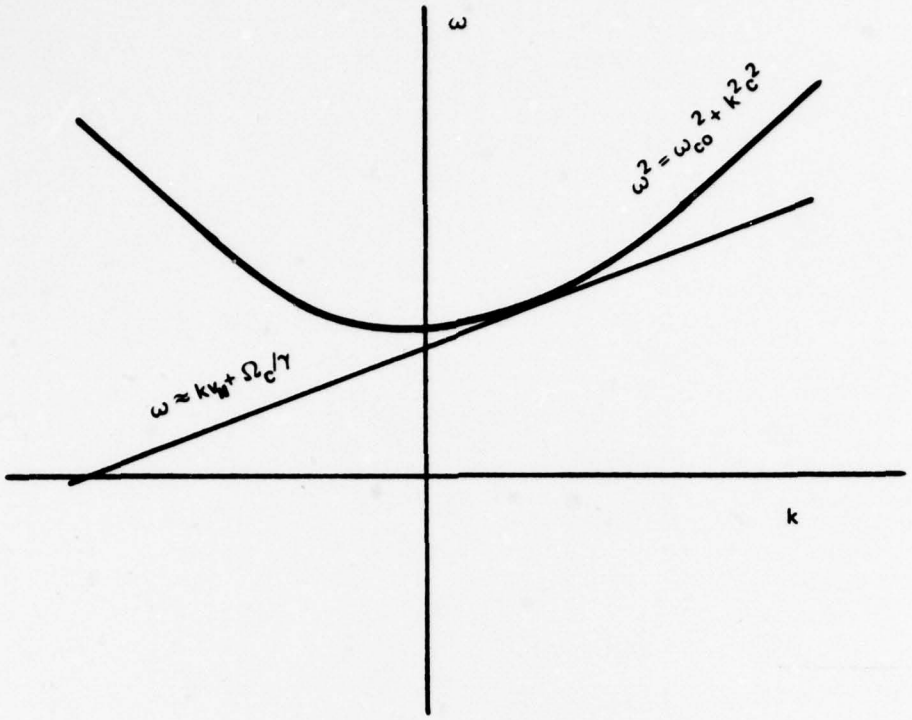

Figure 1.1a. Dispersion curves of the waveguide (upper) and fast cyclotron modes (lower)

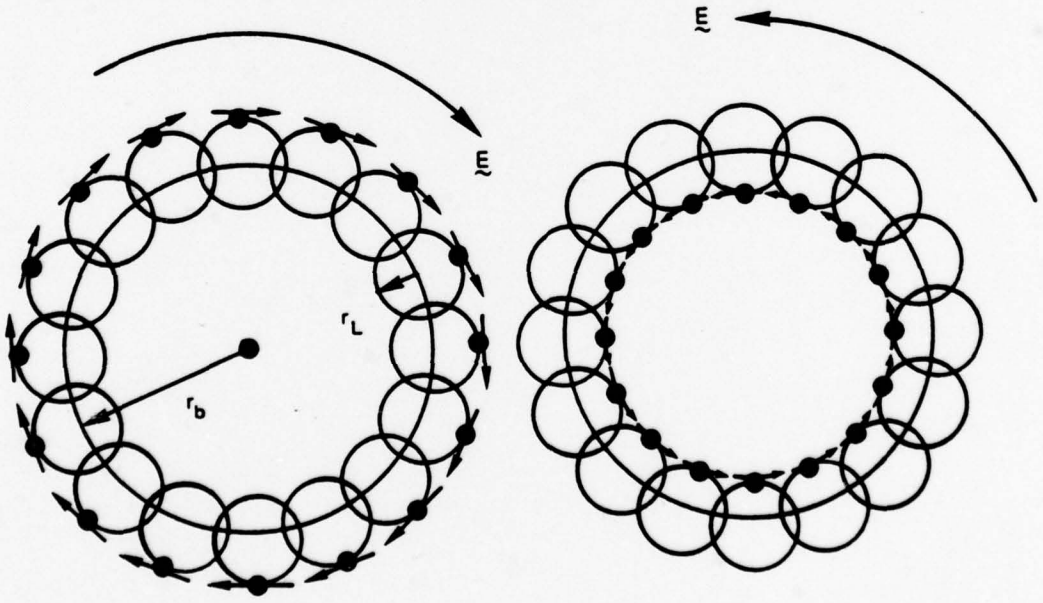

Figure 1.1b. Mechanism of energy transfer from the electrons (dots) of a bunched annular electron beam to the electromagnetic field via the azimuthal electric field. This particular diagram is for the TE_{011}; $\omega \approx \Omega c$. Note that for this interaction the energy transfer is essentially continuous, as the phase of the E_θ field shifts with the change in electron velocity.

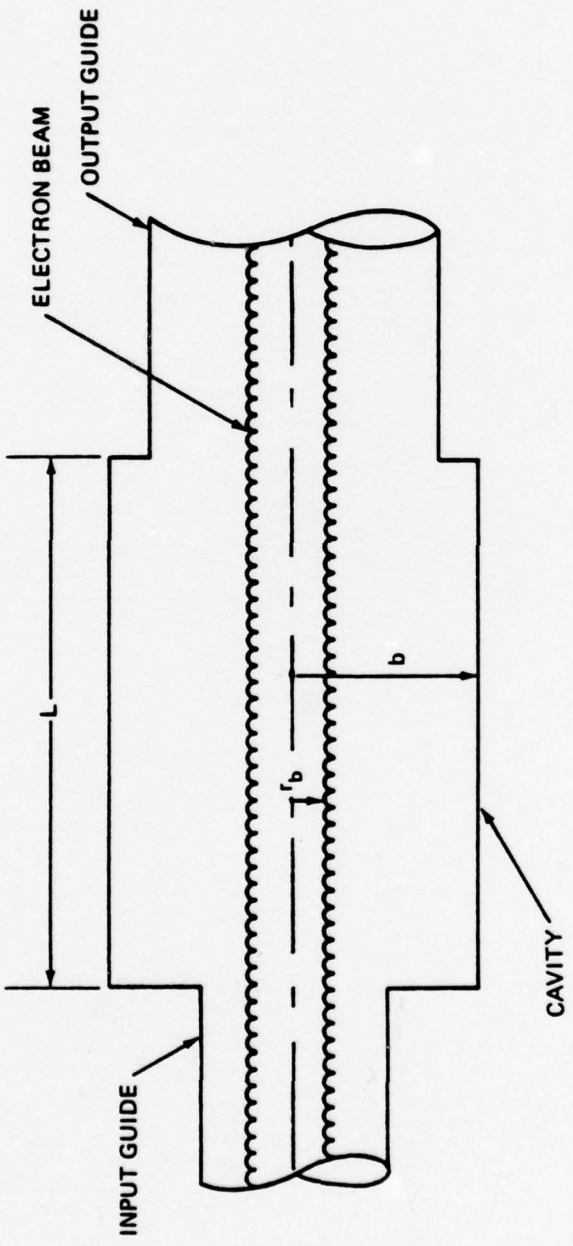

Figure 1.2 Geometry of the cavity and beam in the gyromonotron

An essential point in the linear theory is the coupling coefficient, F, which gives the rate at which energy is transferred from the wave to the electrons. The coefficient is a function of the cavity and beam geometry, the beam energy, current and velocity distribution, the waveguide mode, the harmonic number of the cyclotron frequency, and the phase shift between the beam and waveguide modes. For clarity, we define these parameters below, and discuss them briefly.

b = cavity radius

L = cavity length

r_b = average beam radius

V = beam voltage

β = beam velocity normalized to the speed of light in vacuum, c

P_b = beam power

γ = relativistic factor = $\left[1-(\beta_\perp^2 + \beta_{//}^2)\right]^{-1/2}$

$\alpha = \beta_\perp/\beta_{//}$

m,n,ℓ = radial, azimuthal, and axial eigen-numbers of a cylindrical cavity

s = harmonic number of the magnetic field

$$\Delta = (\omega - kv_{//} - \frac{\Omega_c}{\gamma}) \frac{L}{\beta_{//} c} \qquad 1.3$$

The parameter Δ is the phase shift between the waveguide and beam modes. ω is given by (1.1), k the wave number, is given by

$$k = \frac{\ell\pi}{L} \quad .$$

The parametrical variations in Chu's work that are important in the design methods discussed here are those for the coupling coefficient as a function of the beam radius, and the phase shift. The coupling coefficient is a maximum for certain beam positions; the beam positions required for the maxima are given in the reference [2]. For the $TE_{01\ell}$ mode, with s=1, the optimum beam position is $r_b = 0.47\ b$.

The dependence on the phase shift is most usefully illustrated through a plot of the threshold condition. The threshold condition is defined in terms of the minimum beam power and cavity Q required for oscillation, i.e.,

$$P_b Q \geq (P_b Q)_{th} \qquad 1.4$$

and is inversely proportional to the coupling coefficient. A plot of the threshold $(P_b Q)$ for a cavity used in the 35 GHz oscillator is shown in Figure 1.3.

II. Non-Linear Calculations

While an estimate of the maximum achievable efficiency of an oscillator is possible analytically, an accurate quantitative determination of this parameter has had to be done numerically. A code for determining the energy loss of charged particles due to the interaction with guide electromagnetic fields has been developed by Drobot[1], and modified for use in cavity calculations.

This code utilizes a routine "CYCMASC" which integrates the electron energy loss due to the interaction with the RF fields along a self consistent orbit. The code is 2-dimensional, modeling only azimuthally symmetrical fields and particle distributions.

Fully relativistic equations were used in the code. For these calculations the average amplitude of the electromagnetic field is held constant (in time); i.e., the system is assumed to be in a steady state. The steady state condition is made self consistent by assuming that all of the power lost by the electrons is transferred to electromagnetic fields and radiated, i.e., the system is lossless. The calculation can readily be altered to include cavity losses, which must be considered for very high frequency or low power devices.

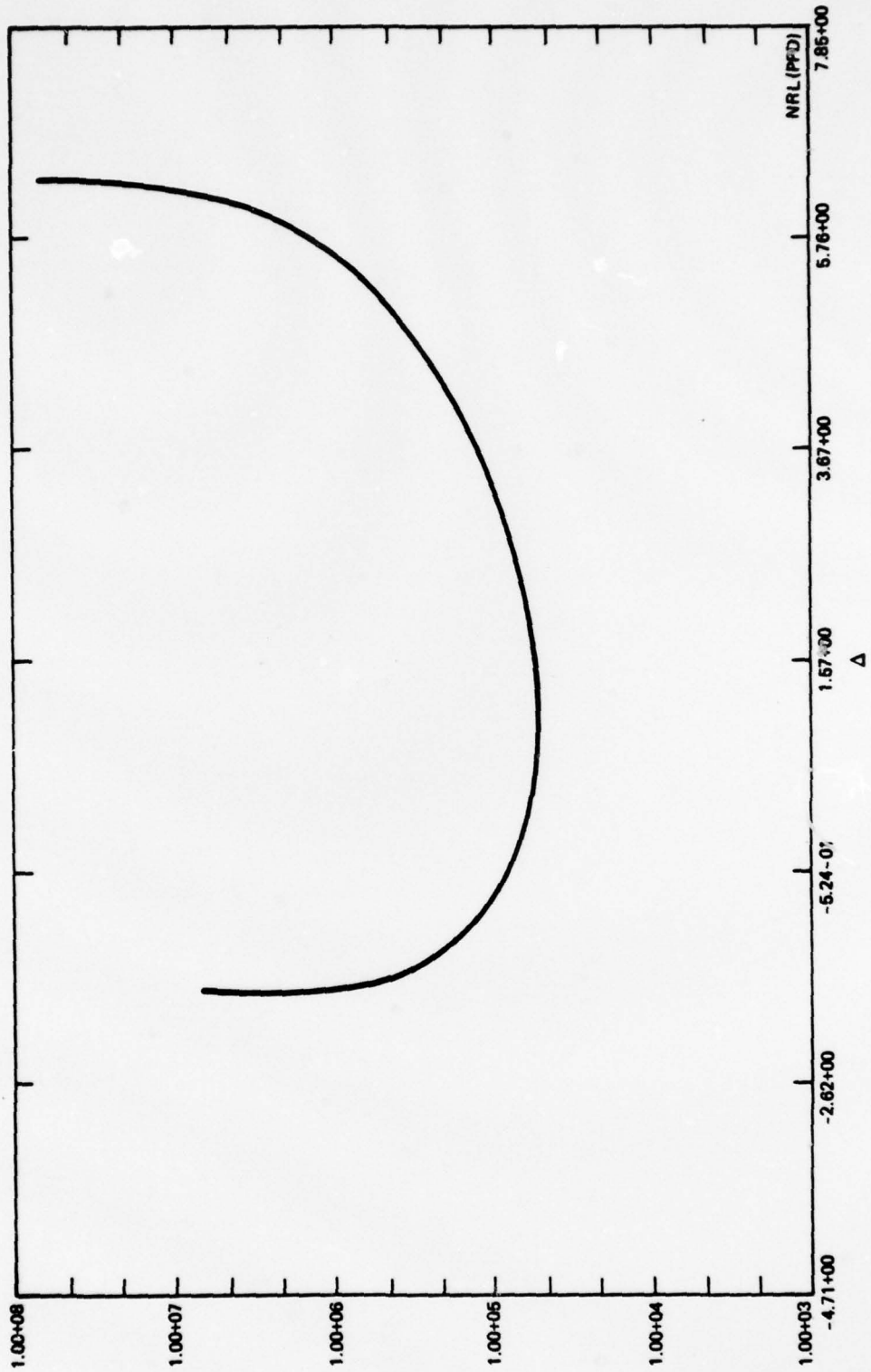

Figure 1.3. Plot of the threshold value for QP_b, in kw, versus the phase shift Δ, for the TE_{011} mode in a cavity with L/b = 5.4, and a beam with γ = 1.14 for α = 1.5.

Inputs to the Code

A simplified flow diagram of the code is given in Figure 2.1.

The inputs to the program are: the initial electron parameters α and γ, the electron beam current, the cavity mode numbers n and ℓ (m=0 always) the shape and magnitude of the RF electric field, the magnitude and shape of the DC magnetic field, and the cyclotron harmonic number s. We will discuss these parameters in detail.

The ratio of perpendicular to parallel electron momenta α, is, as in the linear theory, chosen from electron gun requirements. Clearly it is desirable for α to be as large as possible. However, present gun designs seem limited to maximum α's of 1.5 to 2.0. All of the code runs reported here are for α equal to 1.5. The choice of the total electron energy, given by γ_0, is not so limited. A lower limit to γ_0, may be arrived at through the consideration of the required product of beam power and cavity Q for the initiation of oscillation, derived from the linear theory. This product decreases slowly with decreasing beam voltage, so that, with constant Q, increasing beam currents are required with decreasing γ_0. Eventually the required current will exceed that which can be propagated, and prior to that significant space charge effects may be expected. Chu[2] has given an estimate for an upper bound for a space charge when it is manifested as spreads in the steady state electron energy and parallel velocities. This limit, in terms of a spread in the phase shift Δ, is

$$\delta\Delta = \left(\ell\pi\delta\beta_z + s\,\frac{\Omega_c}{c}\,\frac{L}{\alpha}\,\frac{\delta\gamma}{\gamma_0^2}\right)\frac{1}{\beta} \ll 2.5\pi \,. \qquad 2.1$$

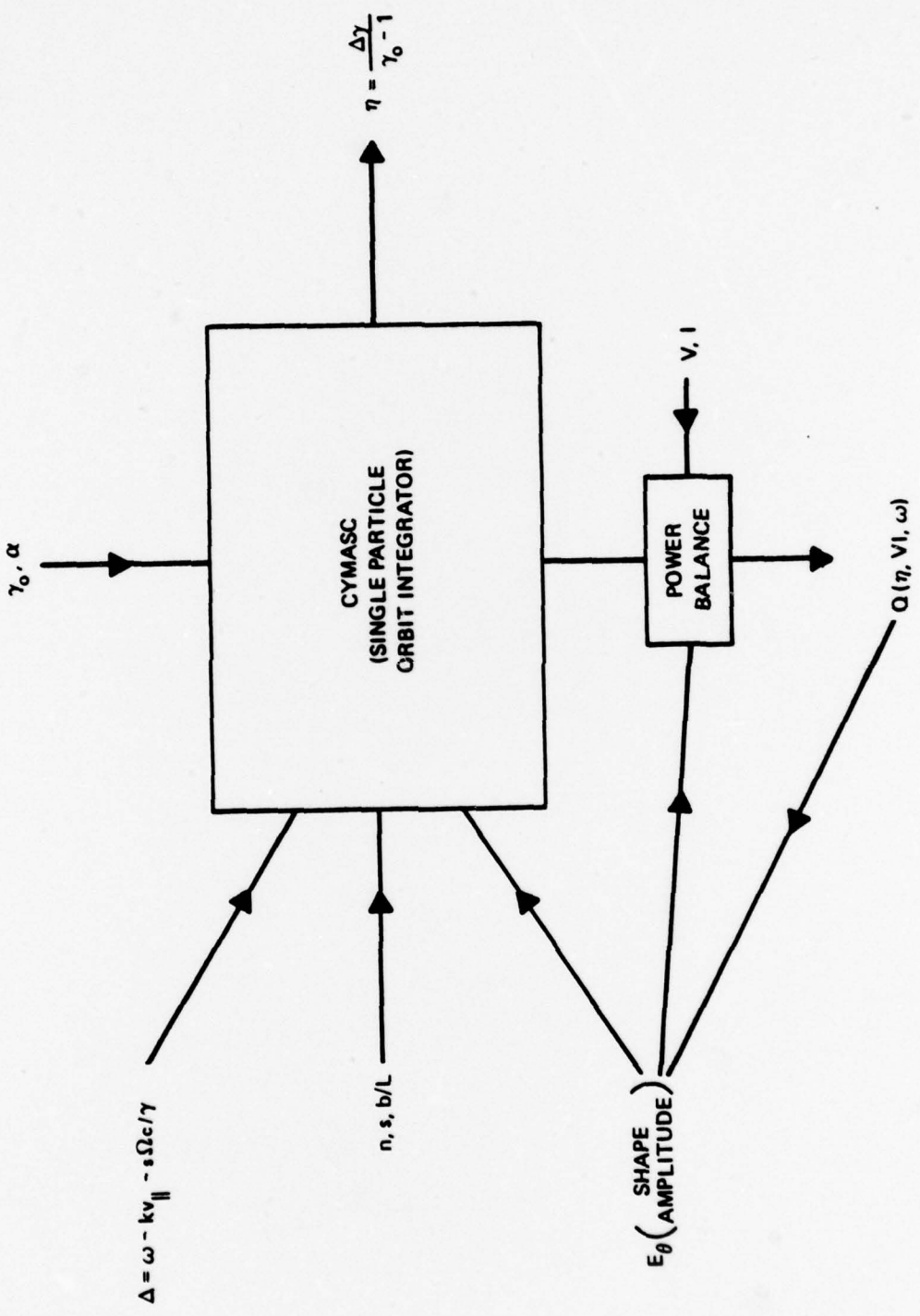

Figure 2-1. Simplified input/output diagram of the code used for the nonlinear calculations of the gyrotron efficiency

The magnitude of the electromagnetic field necessary may be estimated from the requirements that

$$\int E_{eff} \cdot d\ell = \eta(\gamma_0 - 1)\frac{mc^2}{e} \qquad 2.4$$

where the integration is along an electron orbit and E_{eff}, the effective electric field, is given by[2]

$$E_{eff} = \left(\frac{16P\tau}{FLb^2 J_0^2(x_n)}\right)^{1/2} \qquad 2.5$$

where L is the cavity length, $J_0(x_n)$ is the Bessel function of the first kind, and τ is the electron transit time. The coupling coefficient F is given by Chu[2].

The magnitude of the magnetic field can again be estimated from the linear theory. For weak interactions ($\eta << 0.1$) the most efficient operation will be obtained where the beam-wave coupling is maximum. This corersponds to the function F being the most negative, by definition. This will occur in general for the phase shift $\Delta > 0$ where Δ is defined by equation (1.3). For strong interactions, ($\eta > .1$) the electrons will lose energy as they traverse the cavity. For the parameter range of interest Δ will decrease with γ. Assuming that the axial magnetic field is constant, an estimate for the initial Δ that is slightly higher than that for optimum coupling, thereby allowing for some decrease in Δ, seems reasonable. A more effective way to optimize the interaction would be to axially vary the magnetic field, thus holding Δ constant. This will be the subject of a future investigation.

The choice of the harmonic number s is dependent upon the available magnetic field. In most applications it is expected that it will be desirable to use as low a field as possible. This must be balanced against the difficulties caused by the increasing density of competing modes.

Outputs from the Code

The outputs of the code are the efficiency of energy extraction η, and the required Q of the cavity. The efficiency is defined as

$$\eta = \frac{(\gamma_0 - \gamma_f)}{\gamma_0 - 1} \qquad 2.6$$

where γ_0 and γ_f are the initial and final relativistic velocity factors, respectively.

The cavity Q required to achieve the given efficiency is calculated (in the code) using the definition

$$Q \equiv \frac{\omega W_f}{\eta P_b} \qquad 2.7$$

where W_f is the stored electromagnetic field energy. For a right circular cavity and a $TE_{on\ell}$ mode,

$$W = \frac{\varepsilon_0 L E_0^2}{Z} \int_0^b \left[J_1 \left(\frac{p_{on} r}{b} \right) \right]^2 \pi r dr \qquad 2.8$$

where p_{on} is the n^{th} zero of the bessel function J and Z is the characteristic impedance of the cavity.

We note that there is no guaranty that the required Q can be realized in practice. In fact the realizable Q has both an upper and lower bound. The minimum Q achievable is usually termed the diffraction limited Q[3], and is given by

$$Q_{diff} = \frac{\omega \int E_\theta^2 . dV}{v_g \int E_\theta^2 . dA} \approx \frac{4\pi}{\ell} \left(\frac{L}{\lambda_0} \right)^2 \quad (\omega \approx \omega_{co}) \qquad 2.9$$

This is the Q of a smooth waveguide of length L with no reflection at either end. For most cavities considered for gyromonotrons, $L/\lambda > 5$. For a one-half guide wavelength cavity ($TE_{on\ell}$) the diffraction Q is then $\gtrsim 300$. We note that since the area integrals in (2.9) cancel, the diffraction Q is independent of the radial eigen-number (n).

An upper bound for the cavity Q is given by the losses in the cavity walls, i.e., by the ohmic Q. For a right circular cavity with a $TE_{on\ell}$ mode

$$Q_{ohmic} = \frac{\omega\mu\alpha \left[k_{on}^2 + \left(\frac{\pi\ell b}{L}\right)^2\right]}{2R \left[k_{on}^2 + 2\pi^2\ell^2 \left(\frac{b}{L}\right)^3\right]} \qquad 2.10$$

where R is the surface resistance of the cavity walls.
With copper walls the expression becomes

$$Q_{ohmic} = \frac{15.2\sqrt{f}\, b \left(k_{on}^2 + \pi^2\ell^2 \left(\frac{b}{L}\right)^2\right)}{\left(k_{on}^2 + 2\pi^2\ell^2 \left(\frac{b}{L}\right)^3\right)} \qquad 2.11$$

where k_{on} is the n^{th} non-vanishing zero of $J_1(k_{on})$, the Bessel function of the first kind. At 35 GHz a TE_{011} cavity with a radius of 0.5 cm and (b/L) ≈ 0.2 will have an ohmic Q of 14,000.

Results of the Simulations

It is clear from the formulation of the cavity problem that the gyromonotron efficiency is a function of many parameters. Specifically, the efficiency is dependent upon b/L, Δ, E_0, $r_{b/b}$, γ_0, τ, and E_o, and γ_o. As We have examined numerically the effect of variations in b/L, E_0, and γ. As mentioned above, $r_{b/b}$ is chosen analytically. α is assumed to be 1.5, a value deemed reasonable from present electron gun designs.

Usually 32 particles were used in the simulation. Larger numbers of particles were occasionally run as a check, but no significant change in the results was observed. The particles were initially uniformly distributed in phase, but injected into the cavity at the same time. Again, a check was occasionally made on this simplified condition by injecting several groups of 32 particles at different times. No significant change in the code output was observed. The modeling of the beam electrons being initially randomly distributed in phase is justified since the beam is well randomized by the time it reaches the cavity.[5]

The code was checked by comparing its results with those of the linear theory in the regime of low E_θ (low QP), where the linear theory is valid. Agreement was excellent, as can be seen in Figure 2.2.

Output from the code was (in part) in the form of Figure 2.3. This particular output is for a case where strong phase trapping was observed. The large curve is a plot of efficiency vs. axial position. The inserts are plots of the particle perpendicular normallized velocity ($\beta_\perp$) versus phase. As mentioned above, the particles are injected with distributed phase and uniform $\beta_\perp$. Interaction with the cavity field causes bunching and energy extraction from the electrons. (Figures 2.3, b, c). The maximum energy extraction occurs at the axial position $z/_L = \underline{0.72}$. At this point the electrons are well phased trapped. Some particles regain energy as they drift to the end of the cavity (Figures 2.3,d).

Variations of Parameters

The product of the cavity Q and the beam power is proportional to $\omega \int E_\theta^2 \, 2\pi r dr d\ell$ and is therefore, for a given cavity geometry and efficiency, a measure of E_o^2. A plot of η versus QP for b = $\underline{0.53}$ cm (cavity resonant

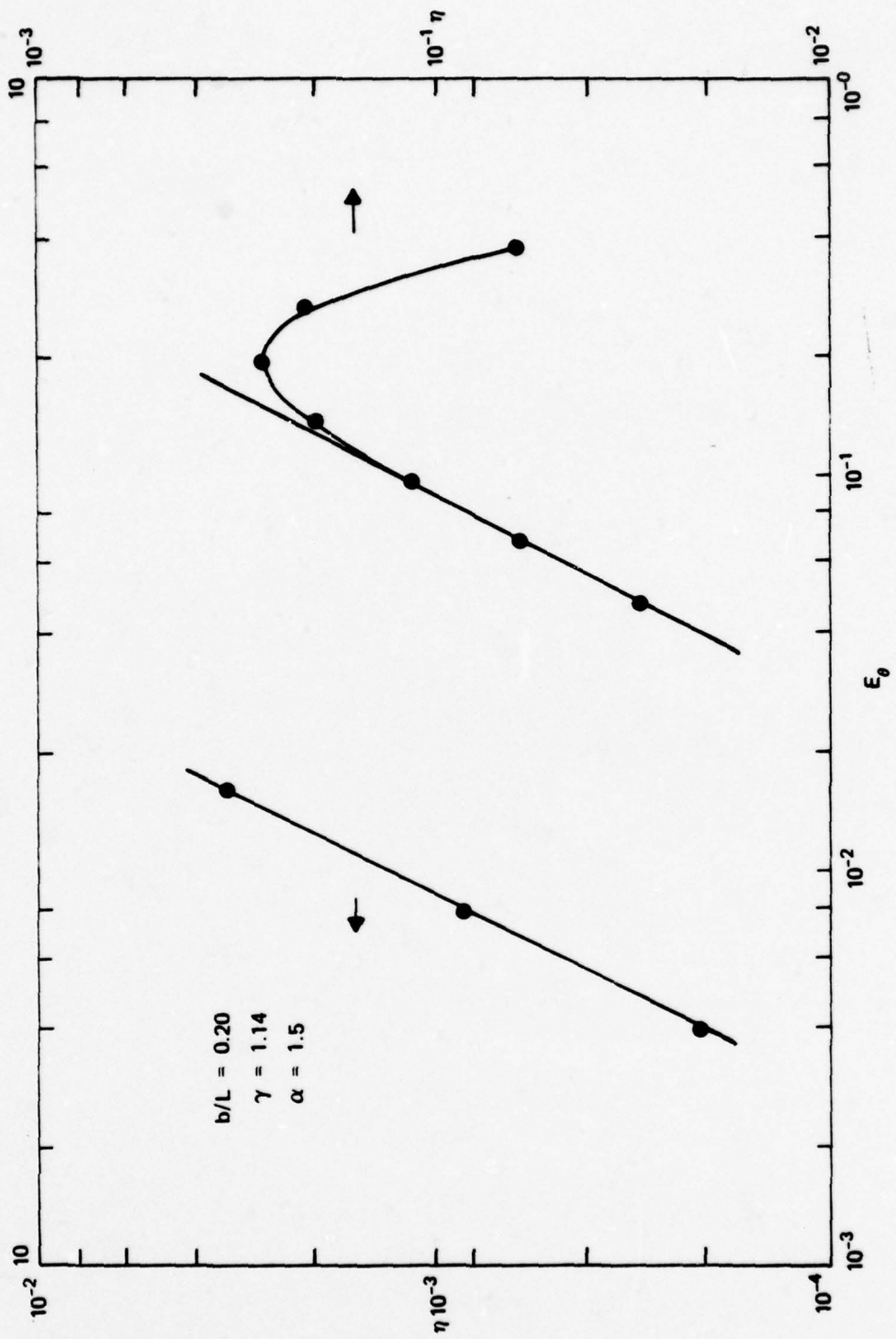

Figure 2.2. Plot of the efficiency versus normallized E_θ as predicted by the linear calculations (solid lines) and the code results (points). Mode = TE_{011}, L/b = 5.0, γ = 1.14, ∝= 1.5.

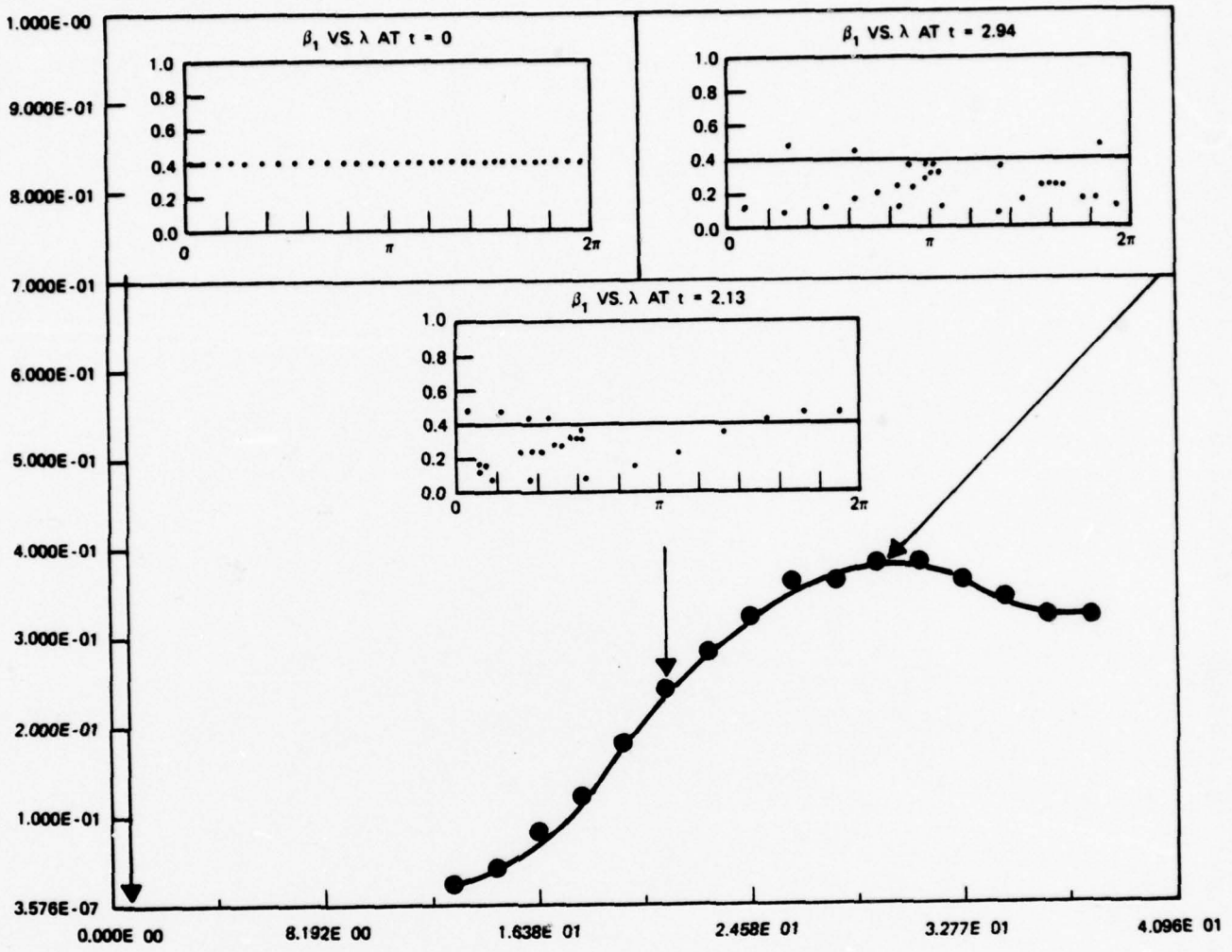

Figure 2.3. Computer output, showing, in the large plot, the gyrotron efficiency versus the number of cyclotron periods an electron has undergone after entering the cavity. The end of the cavity corresponds to the right hand limit of the plot. Note that the efficiency reaches a maximum at Z ≈ .75 L, then drops due to phase trapping. The small plots show the perpendicular velocity (versus azimuthal phase) for three different times. At t ≅ 0, the electrons are unbunched, and all have the same perpendicular energy. At t = 2.13, the electrons are bunched, and most have lost energy, and at t = 2.94, the bunch has started to trap.

frequency equal to 35 GHz) for a TE_{011} mode is given in Figure 2.4. These curves are for cases where the parameter Δ has been adjusted for optimum efficiency. It is observed that an optimum occurs for each L/b, with these optima increasing with this ratio. The Q required for optimum efficiency decreases $E_\theta d\vec{\ell}$ with L/b. This is consistent with the concept that there is an optimum $E_0.d\vec{\ell}$, below which not all available energy has been extracted from the electrons, and above which phase trapping occurs. The effect of trapping can be seen in the cyclic nature of the curves for $\frac{L}{B} = 11$ and $\frac{L}{B} = 7.8$. A corresponding bounce is observed on the η vs. z curve for simulation runs for high values of QP.

η vs Δ

It is expected that for weak (i.e., low efficiency) interactions the optimum initial Δ should be equal to that giving the strongest linear coupling coefficient. In these interactions Δ will remain essentially constant as the electron traverses the cavity, since γ remains almost unchanged (see equation 1.3). For higher efficiency interactions there will be a significant drop in γ s an electron crosses the cavity, and a corresponding decrease in Δ. In order to maintain Δ in the range where strong negative coupling results for the maximum time it is necessary to increase the initial phase shift from the optimum linearly calculated value (see Figure 2.5).

η vs γ

An estimate for the dependence of the efficiency on the beam energy can be derived by noting that energy can be extracted from the electrons while $-0.5\pi \leq \Delta \leq 2\pi$. The resulting expression for the efficiency,[2]

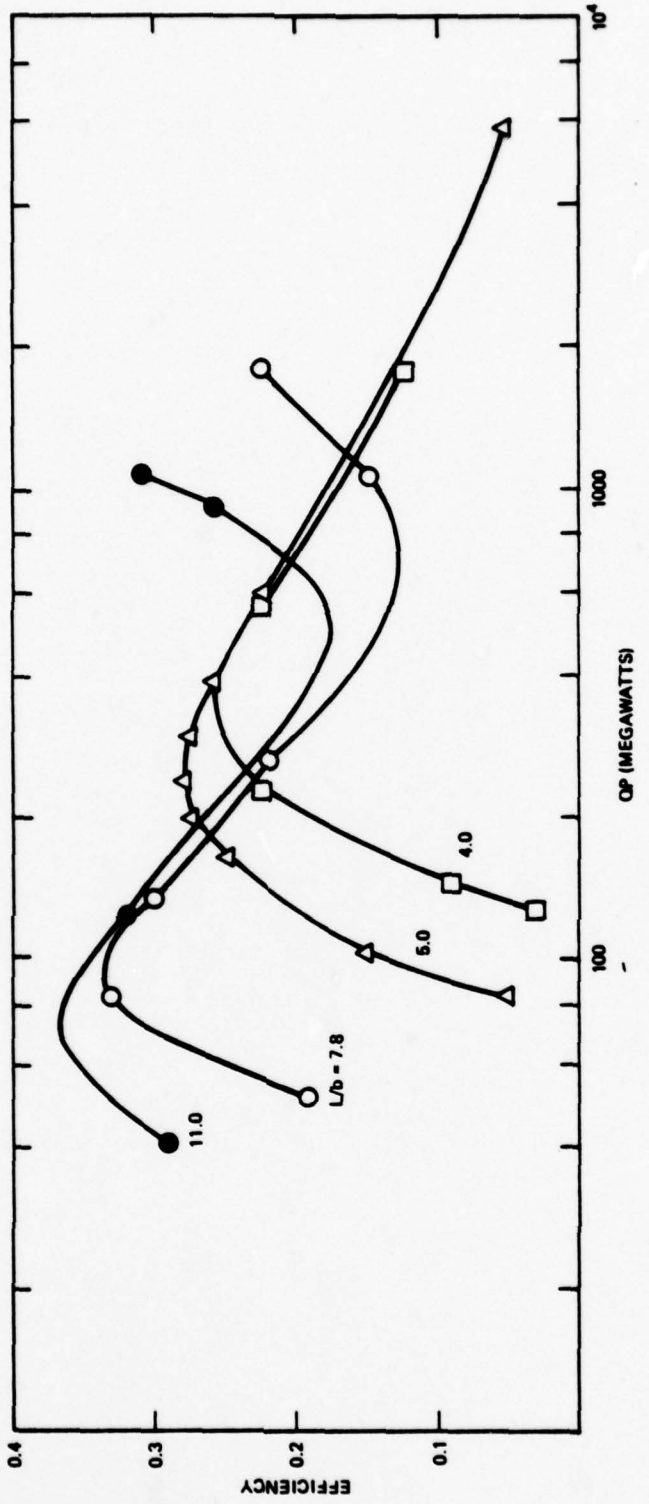

Figure 2.4. Plot of electronic efficiency versus QP for various ratios of L/b. The phase shift, Δ, has been optimized for each point. The connecting lines have been added for clarity, only, and extrapolations have been made by eye.

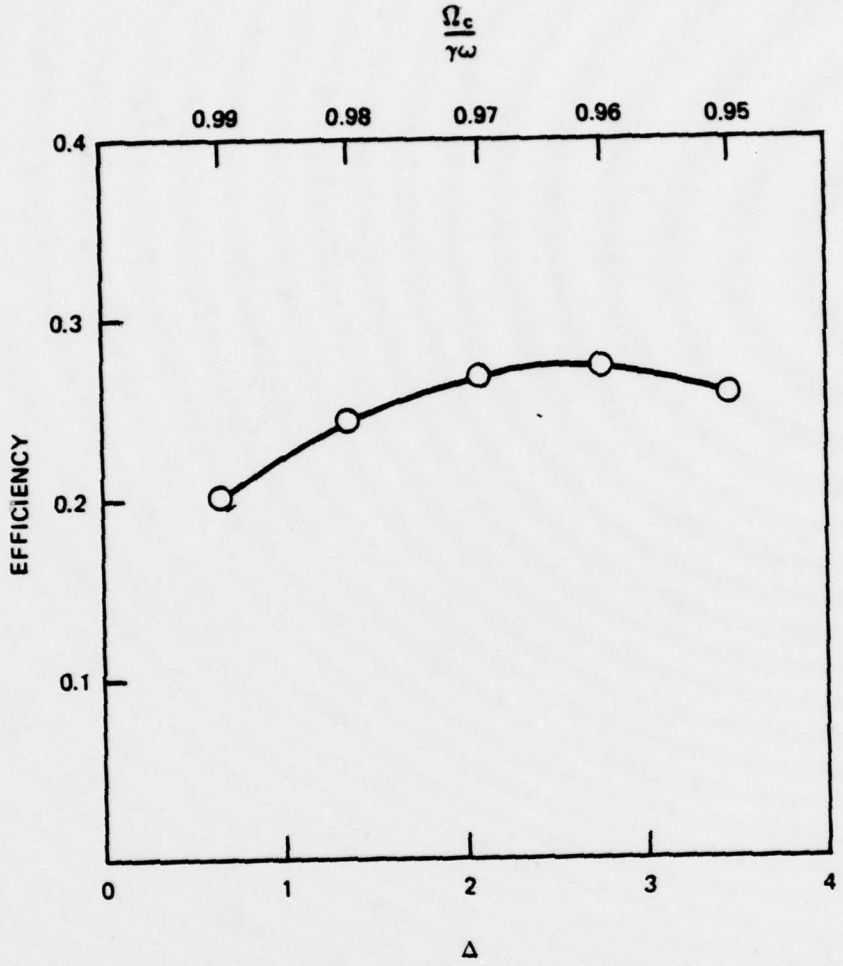

Figure 2.5. Plot of the electronic efficiency versus the phase shift Δ, and the corresponding detuning in magnetic field, given as $\frac{\Omega c}{\gamma}$ over the operating frequency ω. TE_{011}, $L/b = 5.0$, $QP_b = 250$, $\gamma = 1.14$, $\alpha = 1.5$.

$$\eta \leq \frac{2.5\pi\gamma_0\langle\gamma_f\rangle}{s\Omega\,\tau\,(\gamma_0-1)} \qquad 2.12$$

is only an upper bound, and depends on one's estimate for the average of electron energy at the end of the cavity ($\langle\gamma_f\rangle$). In many designs γ_0 and $\langle\gamma_f\rangle \simeq 1$. Here the dominant variation in η will come from the term (γ_0-1). In this case η decreases with increasing γ_0. Simulation results qualitatively confirm this dependence, as is shown in Figure 2.6.

η vs. s

Equation 2.9 predicts a constant efficiency for constant s Ω_c. Therefore, ignoring the effects of temperature, space charge, and competing modes, it would appear that operating at harmonics of the cyclotron frequency causes no reduction in efficiency. This appears to be essentially correct at higher voltages. ($\geq$ 30 kv) as is shown in figure 2.6. However, it is expected that space charge and temperature effects will become more important with increasing s.

Field Shape

The shape of E_θ, as a function of z, can be entered into the code, either point by point, or by a function. As mentioned above, E_θ was normally taken as

$$E_\theta = E_{\theta_0} \sin \frac{\ell\pi z}{L} \quad .$$

However, for one cavity (L/b = 7.8), the field measured for a slightly tapered version was used for E_θ, and the efficiency found. The field profile is shown in Figure 2.16. The maximum efficiency found was 37%, versus 34% for the equivalent untapered cavity. Since no other profiles were run, it is not known whether the electric field profile chosen was an optimum one, and perhaps even larger increases in efficiency might be obtained with different profiles.

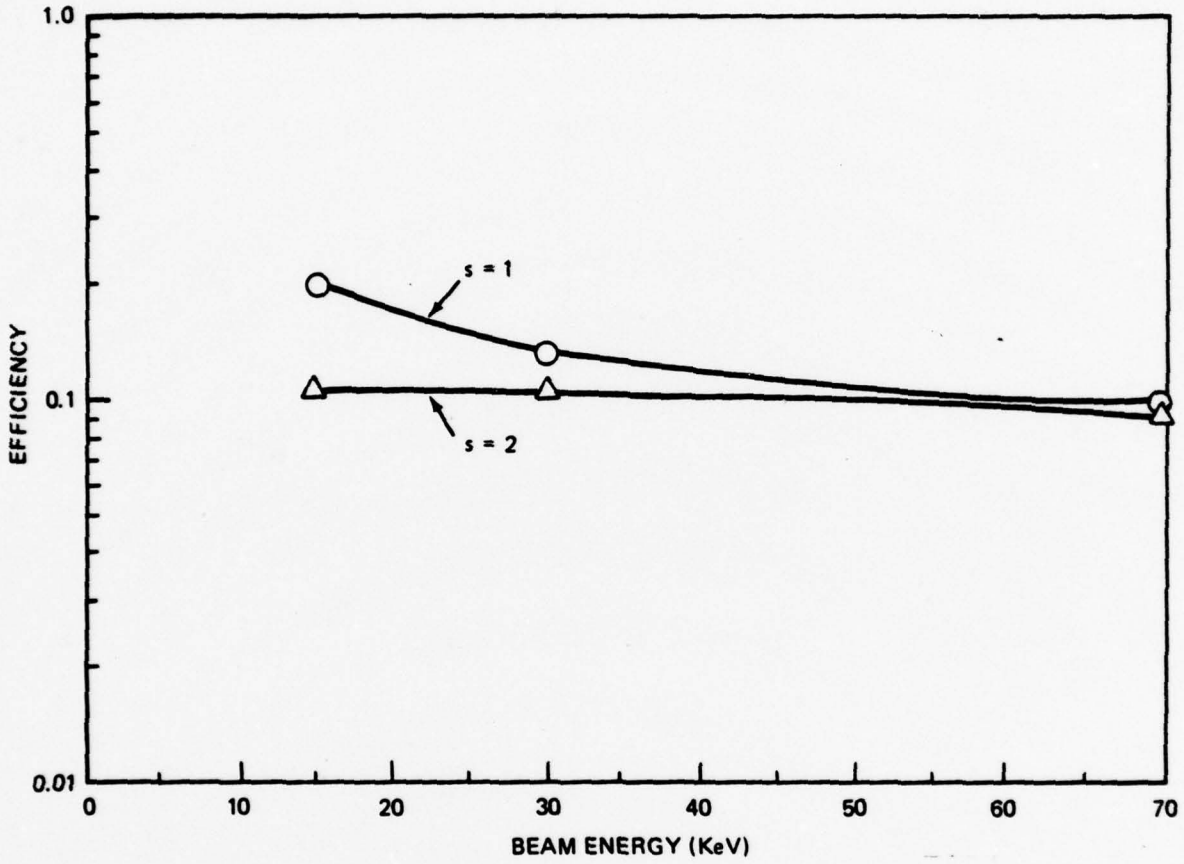

Figure 2.6. Plot of the efficiency versus beam energy, for two values of the cyclotron harmonic numbers. Mode = TE_{051}, L/b = 8, α = 1.15; QP and Δ are optimized for each point.

The reason for the increase in efficiency is not all together clear. A possible explanation is that the slow rise of the field at the entrance of the cavity promotes better (more adiabatic) bunching, and that the more abrupt drop of the field at the output reduces phase trapping, as can be observed in Figure 2.2.

Design Procedures

As has been shown in the above sections, the efficiency of a single cavity gyrotron oscillator is a function of many variables. These variables are interdependent, and are bounded by external constraints. We present here by illustration a rough method by which an optimum design can be achieved, with the various constraints discussed above.

Figure 2.7 gives an outline of the order of calculations necessary for the design. The first column contains the independent variables, of which f, P, s, and L are assumed to be determined by desired output characteristics (f, P) or given system characteristics (s, r, P). The parameters in parentheses are ones which must be varied in order to achieve an optimum (and feasible) design.

The second column contains those quantities which can be calculated by analytic methods. The third column has conditions which, although not final design parameters, must not exceed given bounds in order for the design to be feasible. The fourth column contains those qualities which are determined using the code *CYCMASC*. The last column holds the final design parameters.

35 GHz Oscillator Design

Parameter specifications

The above procedures were used to design the 35 GHz oscillator. For this device, it was intended that the design incorporate an electron gun designed

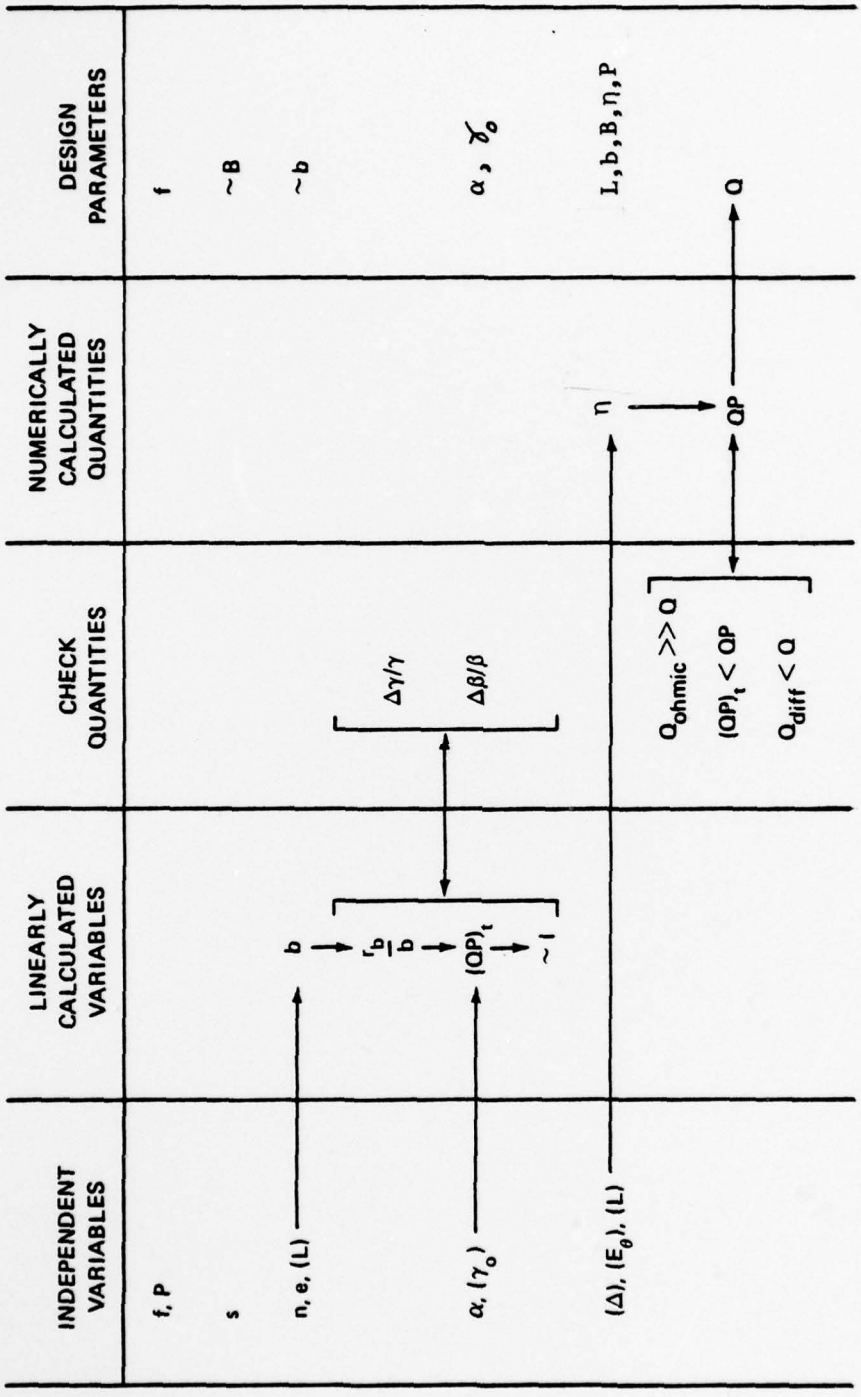

Figure 2.7. Outline of the procedure used for a gyromonotron design. See text for explanation.

for a gyrotron amplifier. The beam parameters for this gun were

$$V = 70 \text{ kv}$$

$$I \leq 10A$$

$$\alpha \cong 1.5$$

For simplicity of operation and for ease of handling of the output radiation, the azimuthal eigen-number n was chosen to be 1. The axial eigen-number was initially chosen to be 1, since it was expected that the TE_{011} mode would have a lower starting power than the $TE_{01(2,3,4...)}$ modes. This point was validated by the simulation runs, and is discussed below.

r/b was mentioned in section 1, and is optimally 0.47. (For the TE_{011} case the radius of 0.47b corresponds to the position of the peak of the electric field.)

Calculation of the space charge parameters, using equations 2.1, 2.2, and 2.3, yields

$$\Delta\gamma/\gamma = 2.9 \times 10^{-3}$$

$$\Delta\beta_z/\beta_z = 4.13 \times 10^{-2}$$

$$\left(\ell\pi\ \Delta\beta_z + \frac{s\Omega_c}{c}\ \frac{L\delta\Delta}{\gamma_0^2}\right)\frac{1}{\beta_{zo}} = 0.33$$

We note that this last quantity is much less than 2.5π, thus meeting Chu's criterion for the effects of space charge to be negligible.

Using the graphs of Figures 2.4 and 2.5, we find the optimal values for L/b, Δ, and QP. It is clear from Figure 2.4 that the efficiency increases monotonically with the ratio L/b. Concommitantly, however, a decreasing value of QP_b is required to achieve the optimum efficiency for that ratio. For a given beam power, QP_b has the lower bound of $Q_{diff}P_b$, where Q_{diff} is given

by equation 2.9. Thus there will be a finite optimal value for L/b. This point is illustrated by Figure 2.8. For ρ equal to 0.75, the optimum value for L/b is 5.4, and the optimum QP_b is 1.5×10^6.

The maximum efficiency yielded by the code for these values of input parameters is 27%. The magnetic field which yields this efficiency is approximately 13.53 kg and the corresponding phase shift, Δ, is 2.8.

The threshold value for QP_b is found to be approximately 6×10^7. The operating QP is 2.5 times this value, and is thus satisfactory from this standpoint.

The final design parameters are listed in table 2.1. Note that the gyrotron will have an output power of 150 kw at the peak efficiency of 27%. The NRL electron gun is capable of producing a beam of up to 15A (for short periods), thus an output power of 268 kw can be achieved, but at lower efficiency (see Figure 2.9). Note that these characteristics are all for an untapered cavity. For a slightly tapered cavity, we might expect an efficiency of $\approx$ 30%, with an output power of 168 kw.

Competing Modes

One consideration not discussed above is that of competing modes. All of the previous analysis is made on the assumption that only the desired mode will be excited. A mode of the system exists only when there is a near intersection of the beam and waveguide dispersion relations; i.e., when the phase velocities are almost equal. For the 35 GHz oscillator, the dispersion relations for the TE_{011} and neighboring $TE_{01,2,3,4...}$ modes are given in Figure 2.10. For any of these modes to oscillate it is necessary that the threshold QP_{beam} (for the mode of interest) to be above that of the system. Only the analysis of azimuthally symmetric modes has been done, and thus the

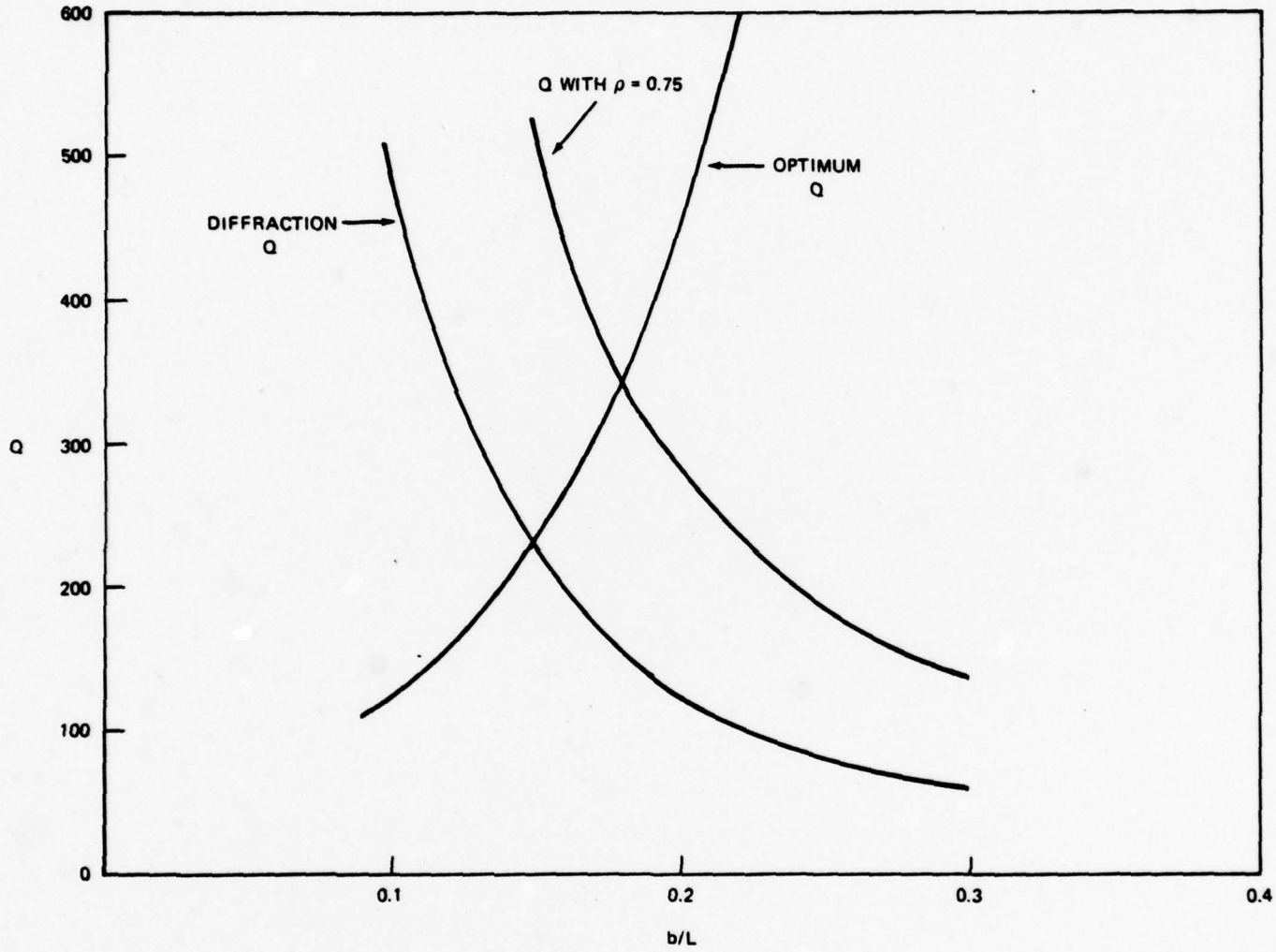

Figure 2.8. Obtainable and optimum Q's versus the ratio b/L.

TABLE 2.1

GYROMONOTRON DESIGN PARAMETERS

Beam Energy		70 kV
Beam Current		8 Amps
Frequency		35.0 GHz
Cavity Mode		TE_{011}
Output Mode	(without converter)	TE_{01} (circular)
	(with converter)	TE_{10} (rectangular)
Cavity Q		390*
Cavity Length		2.85 cm
Max. Cavity Radius		0.530 cm
Efficiency		27%
Output Power		151 kw

*Value determined in cold test.

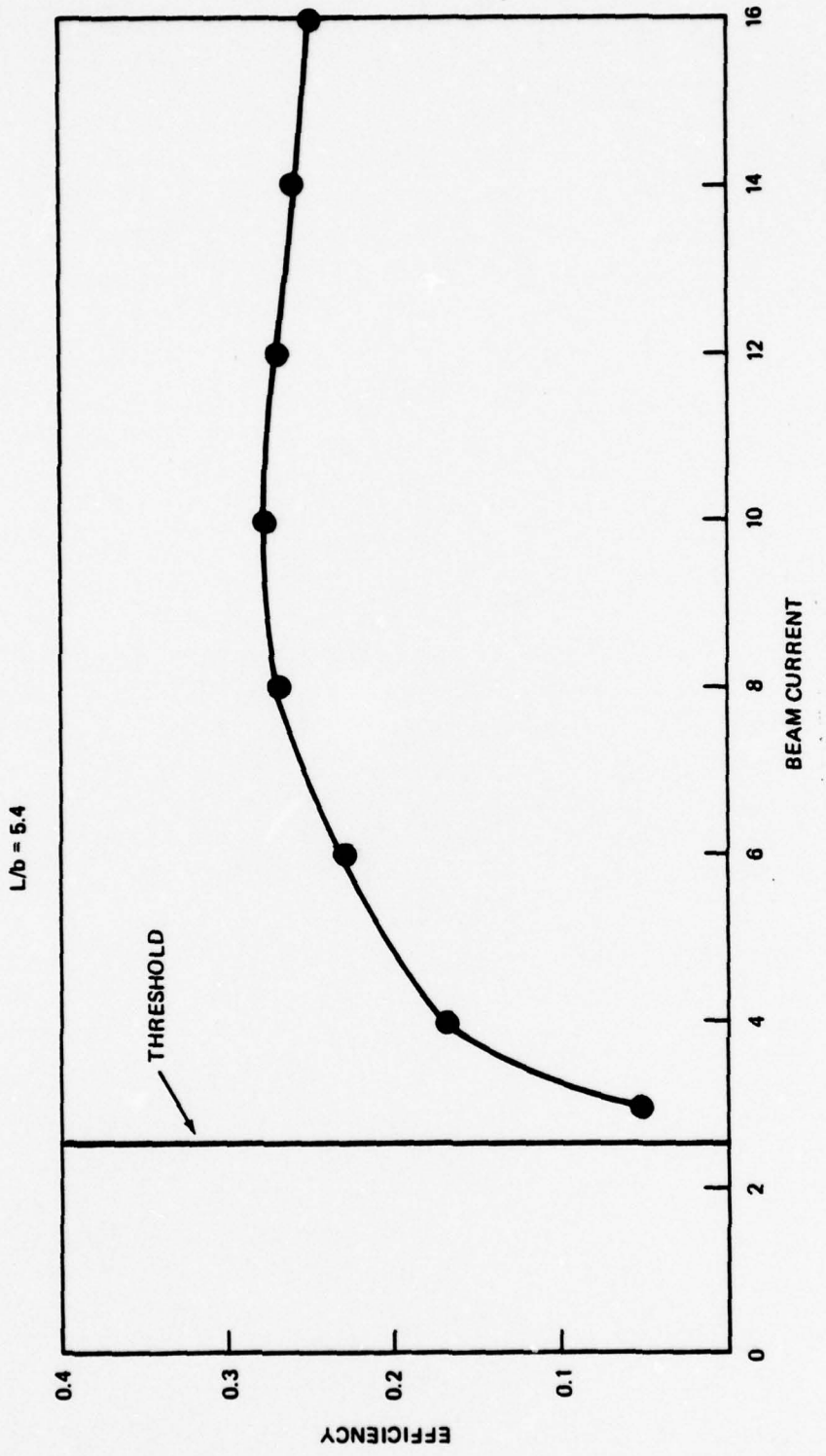

Figure 2.9. Plot of efficiency versus beam current. Q = 390, V = 70 kv, α = 1.5, L/b = 5.4, TE_{011} mode. Δ is optimized for each point.

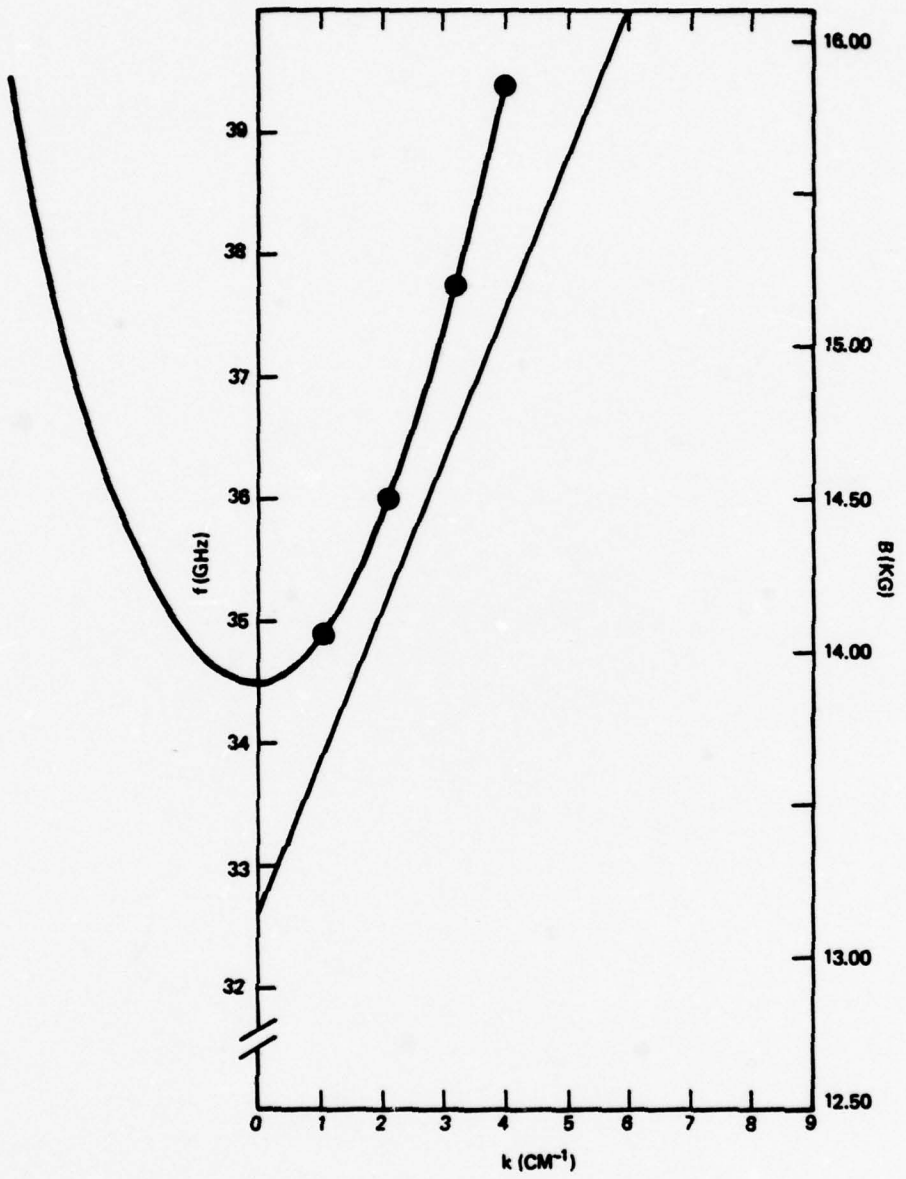

Figure 2.10. Dispersion curve for the gyromonotron with parameters specified in Table 2.1. The operating mode is the TE_{011} - most likely competing modes are the $TE_{01,2,3...}$. These modes are shown as dots on the waveguide curve.

threshold condition can be determined only for these modes. However, from symmetry considerations, it is expected that the interaction for S-1 will be strongest for the $TE_{on\ell}$ modes. Additionally, non-azimuthally symmetric modes may be preferentially suppressed by interrupting or loading axial wall currents, which are not present in the $TE_{on\ell}$ modes.

For the 35 GHz oscillator, the modes which look most likely to compete with the TE_{011} mode are the $TE_{01\ell}$ modes, where $\ell = 2,3,4\ldots$. The minimum threshold values of QP_b, for these modes are given in Table 2.2. Also given are the threshold values for the magnetic field at which the maximum efficiency is expected for the TE_{011} mode. The difference between these values results from the fact that the minimum in the threshold QP_b occurs at a different phase shift for each mode. We note that strong mode competition would be expected if the Q for all modes were equal. Fortunately, Q is expected to go as

$$Q = \frac{Q_{diff}}{1-\rho^2} \qquad 2.9$$

where $$Q_{diff} \cong \frac{4\pi}{\ell}\left(\frac{L}{\lambda_0}\right)^2$$

and $$\delta \cong \frac{(f^2-f_{co}^2)^{1/2} - (f^2-f_{cc}^2)^{1/2}}{(f^2-f_{co}^2)^{1/2} + (f^2-f_{cc}^2)^{1/2}} \qquad 2.13$$

f_{co} and f_{cc} are the cutoff frequencies of the output guide and cavity, respectively. Q is therefore a strongly decreasing function of ℓ, and the minimum separation will be $Q(\ell) = \frac{1}{\ell} Q(1)$, with $\rho = 0$. Therefore, no difficulty is expected from mode completion with this oscillator.

TABLE 2.2

THRESHOLD VALUES FOR QP_b FOR

$TE_{01\ell}$ MODES

35 GHz CAVITY

ℓ	$(QP_b)_{min}$	$(QP_b)_{\Delta = 2.8}$
1	6×10^7	9.5×10^7
2	7×10^7	8×10^7
3	8.5×10^7	8.5×10^7
4	1×10^8	1×10^8

In leaving this subject, we note that although the problem of competing modes does not seem serious for a gyrotron operating in the TE_{o11} mode with s = 1, it may prove to be a limiting factor in devices with higher mode numbers.

Mechanical Design

The mechanical design of the 35 GHz oscillator was prepared with the goal of producing a device that was as simple and flexible as possible, and that could be fabricated in the NRL shops. The former concern reflects the desire that the cavity and other microwave structures (such as the transition from the cavity to the output guide) be easily replaceable. For this reason, the microwave interaction structures were mounted in a vacuum shell, thus removing the requirement that joints between the structures be vacuum tight.

The second concern is not trivial. Vacuums of 10^{-8} to 10^{-7} torr are required for operation of the electron gun. The residual gases must also be free of sutstances which will contaminate the cathode. Principal among these substances is zinc, which is a component of all hard solder which can be used with a torch. This difficulty can be eliminated by brazing materials in a hydrogen or vacuum oven. Although such facilities existed at NRL, there were no trained personnel to operate them. Therefore, it was decided to make all parts of stainless steel, and weld all joints. This method has worked reasonably well for laboratory experiments.

The oscillator is shown in Figure 2.11. We shall discuss each component in order, from left to right.

Electron Gun

The electron accelerator is of NRL/Varian design[5,6], and manufactured by Varian. The design calls for an operating voltage of 70 kv, with a beam

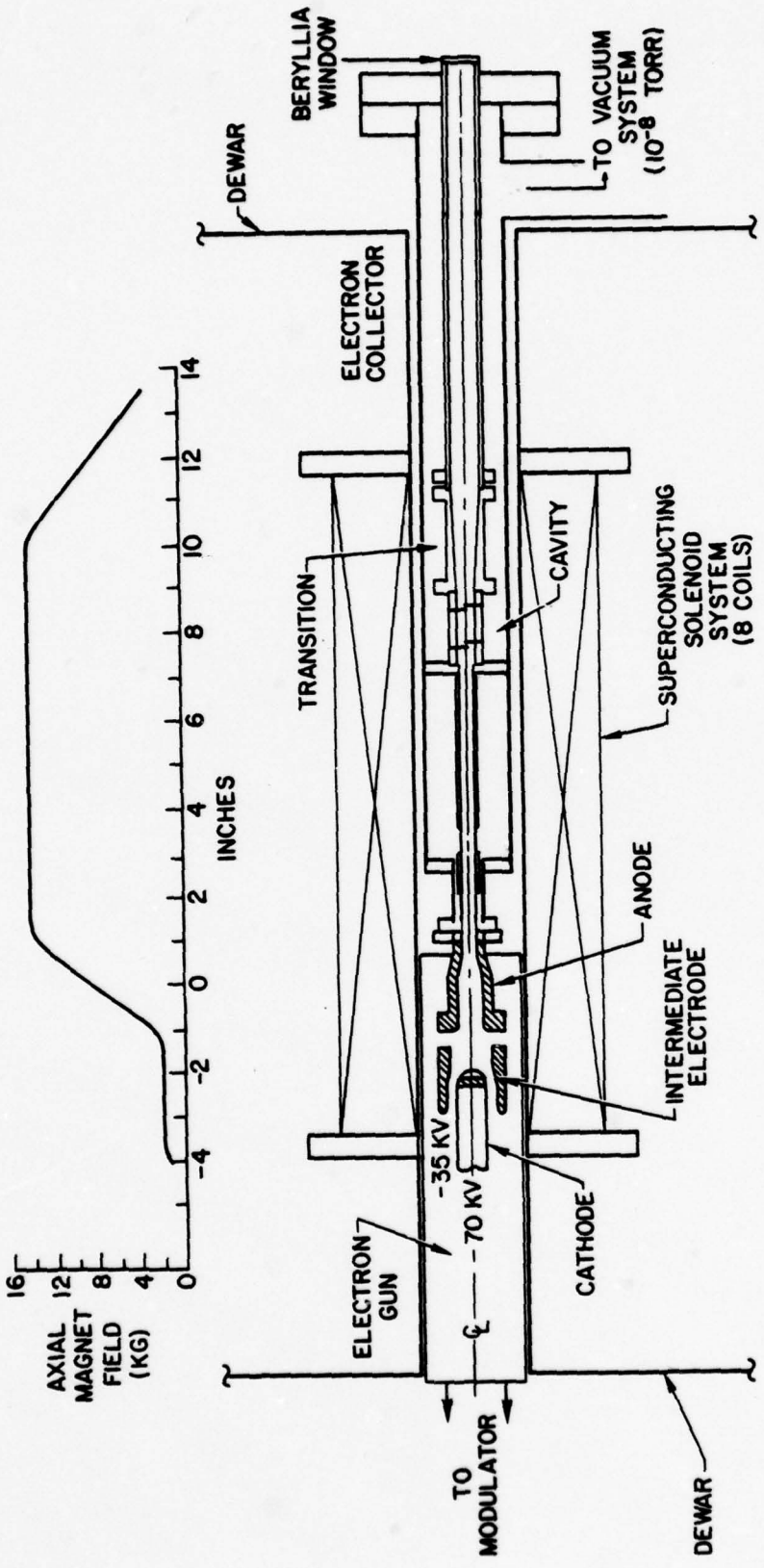

Figure 2.11. Schematic of the 35 GHz gyromonotron

current of 8-10A. Under these conditions, the ratio of perpendicular to parallel electron velocities should be 1.5, and the spread in the parallel and perpendicular velocities to be 10% and 7%, respectively. Chu[2] estimates that these spreads should not significantly effect the maser mechanism.

Beam Input Guide

The guide diameter was chosen to be 0.775 cm (0.305 inches) in order to minimize the possibility of the TE_{21} modes being excited. At 35 GHz, the cutoff diameter for this mode is .802 cm. In light of experiments being conducted at the time of the writing of this report, this may have been an unwise policy, since it appears that a substantial portion of the beam is being intercepted by this guide. The beam outer diameter is specified to be .660 cm (.260 inches), so interception should not take place with careful alignment. There is a question then, as to the actual size and character of the beam, and experiements are being prepared to examine these parameters.

Cavity

Three cavities were fabricated, two with a slight taper, one with no taper. Their dimensions are given in Figure 2.12. We note that cavity #6 is the cavity specified in the design. Cavity #5 was chosen to test the effect of tapering, and cavity #4 was chosen to test the effect of varying L/b.

The input end of the cavities approximated a solid wall, in that the input guide was a strongly cut off guide. The output end of the cavity was defined by an outward step in diameter. This step is a discontinuity in the guide impendance, and thus causes a reflection. For the TE modes, the impedance is lower in the larger diameter guide. Thus the discontinuity looks like a partial "short circuit." The reflection caused by the step is given by equation 2.10. This expression uses the intrisic impedance of a TE wave in an infinitely long waveguide. Since none of the "guides" are uniform

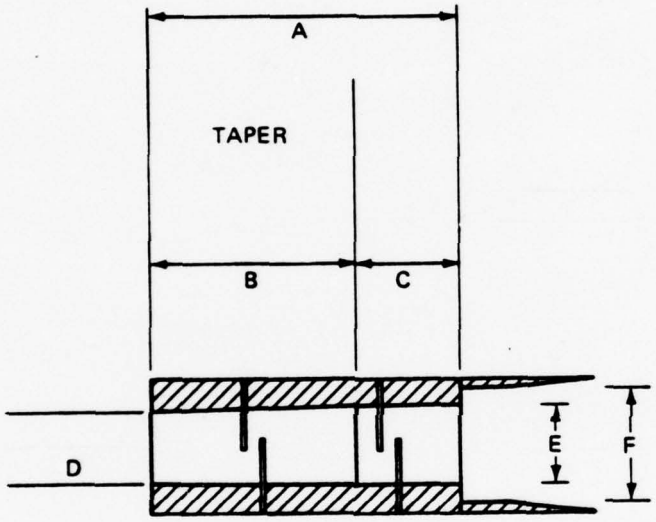

	CAVITY #4	CAVITY #5	CAVITY #6 (NO TAPER)
A	4.313 CM	2.857 CM	2.857 CM
B	2.847	1.887	–
C	1.466	0.970	2.857
D	1.029	1.035	1.053
E	1.052	1.060	1.053
F	1.245	1.245	–

Figure 2.12. Diagram of the cavities used

in the region of interest for more than a few wave lengths, the expression for the reflection coefficient is an approximation and must be checked by cold testing.

The Q resulting from the cavity geometry is given by 2.13. A Q of $\simeq$400 was desired. In order to achieve this value of Q, a step larger than that provided by the output waveguide is demanded by 2.13. However, cold tests indicated that the step sizes given in Figure 2.12 be used. See below for a discussion of this discrepancy.

Output Waveguide and Collector

The output guide was chosen to be a standard circular waveguide size, with a diameter of 1.603 cm (0.631 inches). This guide had approximately fifty 0.159 cm diameter holes drilled in it for pumping. It also serves as a rudimentary collector allowing pulse rates of $\sim$10 pps.

Output Window

Two configurations of output window were designed. Both were one half or three halves wave length resonant windows fabricated from beryllia. Beryllia was chosen as a common microwave window material with high heat conductivity, a property which will be useful in the long pulse gyrotron.

The two windows are shown in Figure 2.13. The first (Figure 2.13a), is designed to be used with the mode converter. With this window, the output waveguide is uniform in diameter from the collector to the mode converter. The second window (Figure 2.13b) is five centimeters in diameter, and was used in conjunction with a horn for radiating the gyrotron output. The reflectance of both of these windows was measured. The results are shown in Figures 2.14 and 2.15.

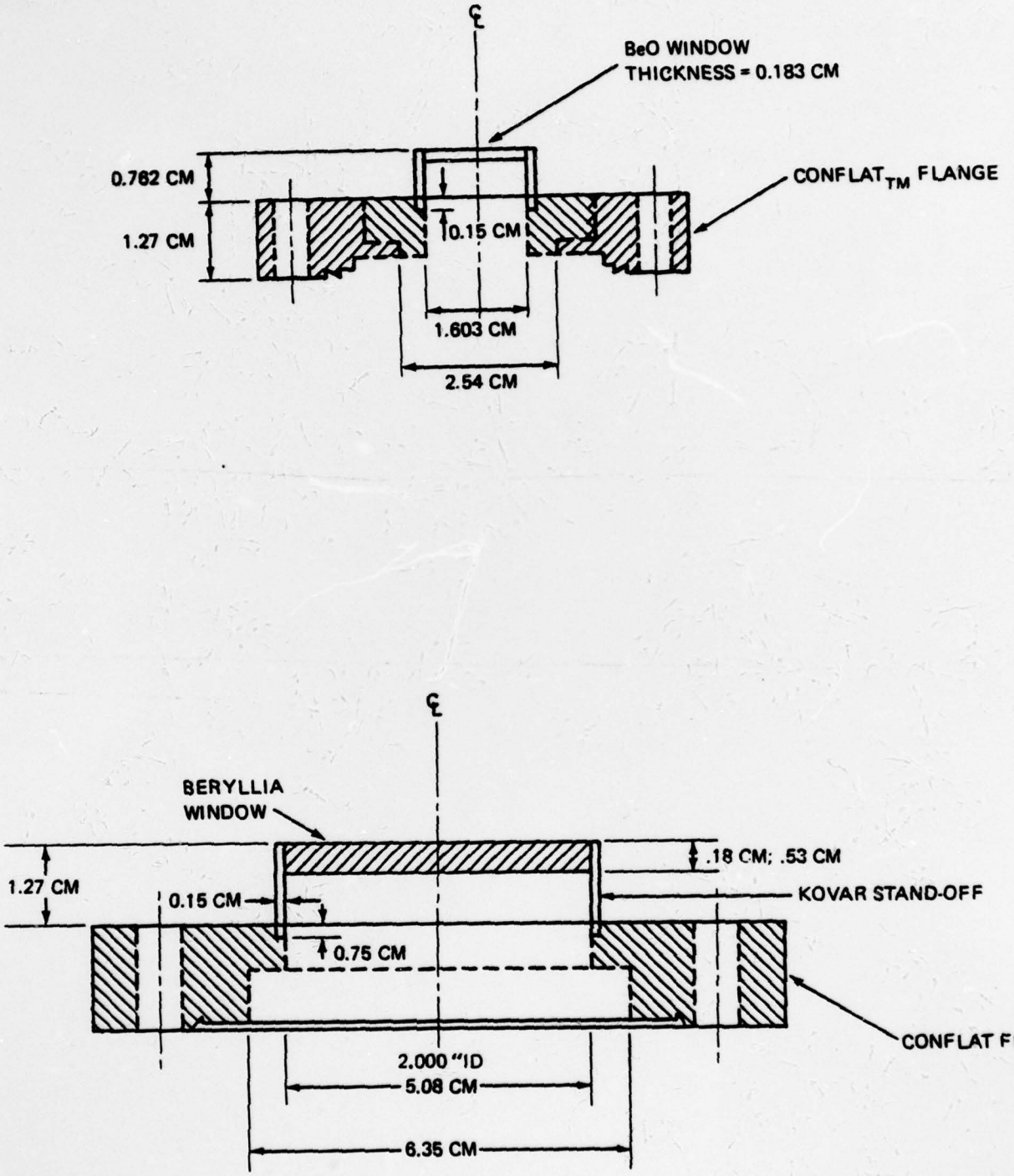

Figures 2.13a and 2.13b. Schematics of two different output window configurations

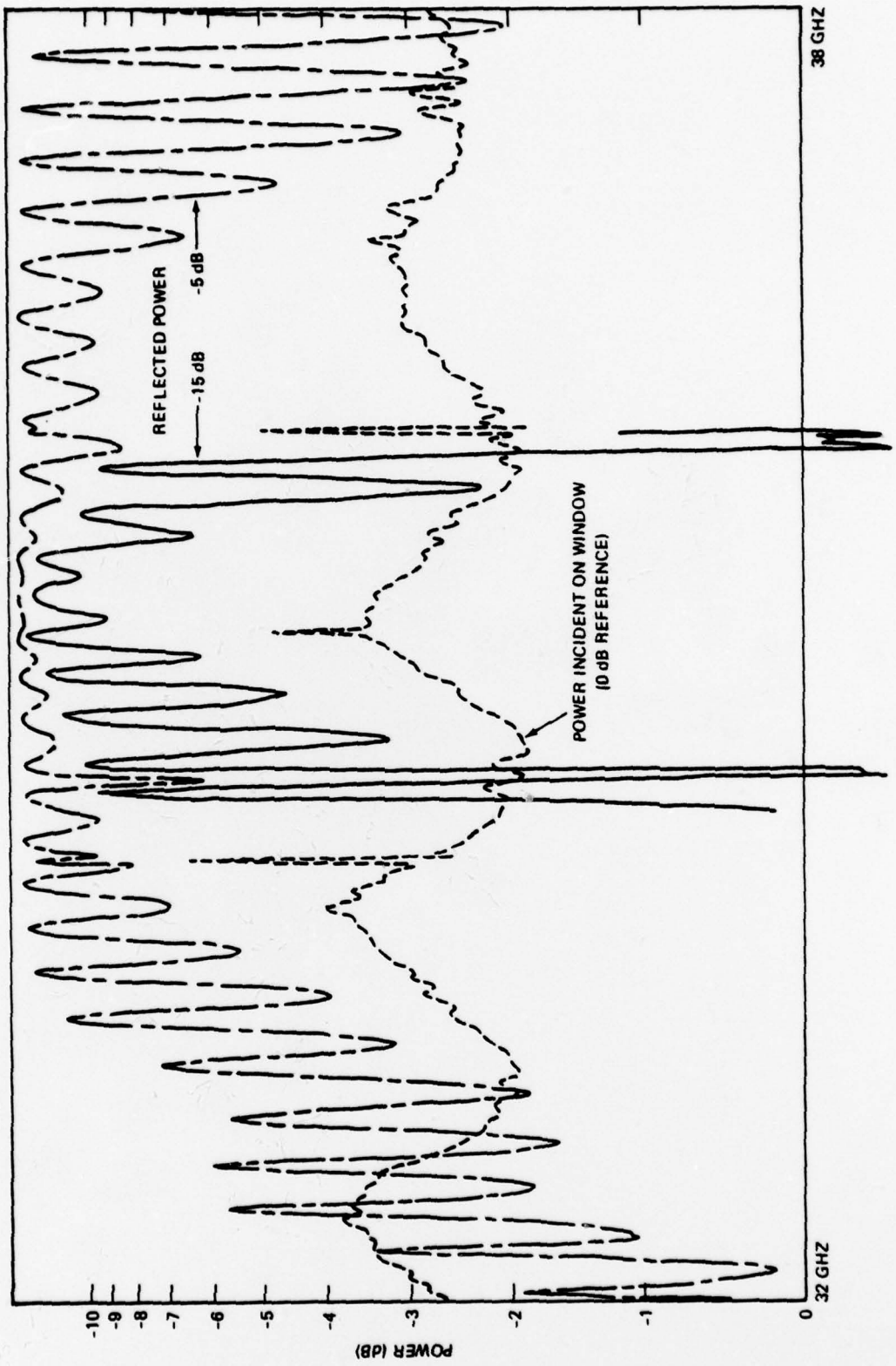

Figure 2.14. Plot of incident and reflected power versus frequency for the small window. The window was tested in place in the output waveguide.

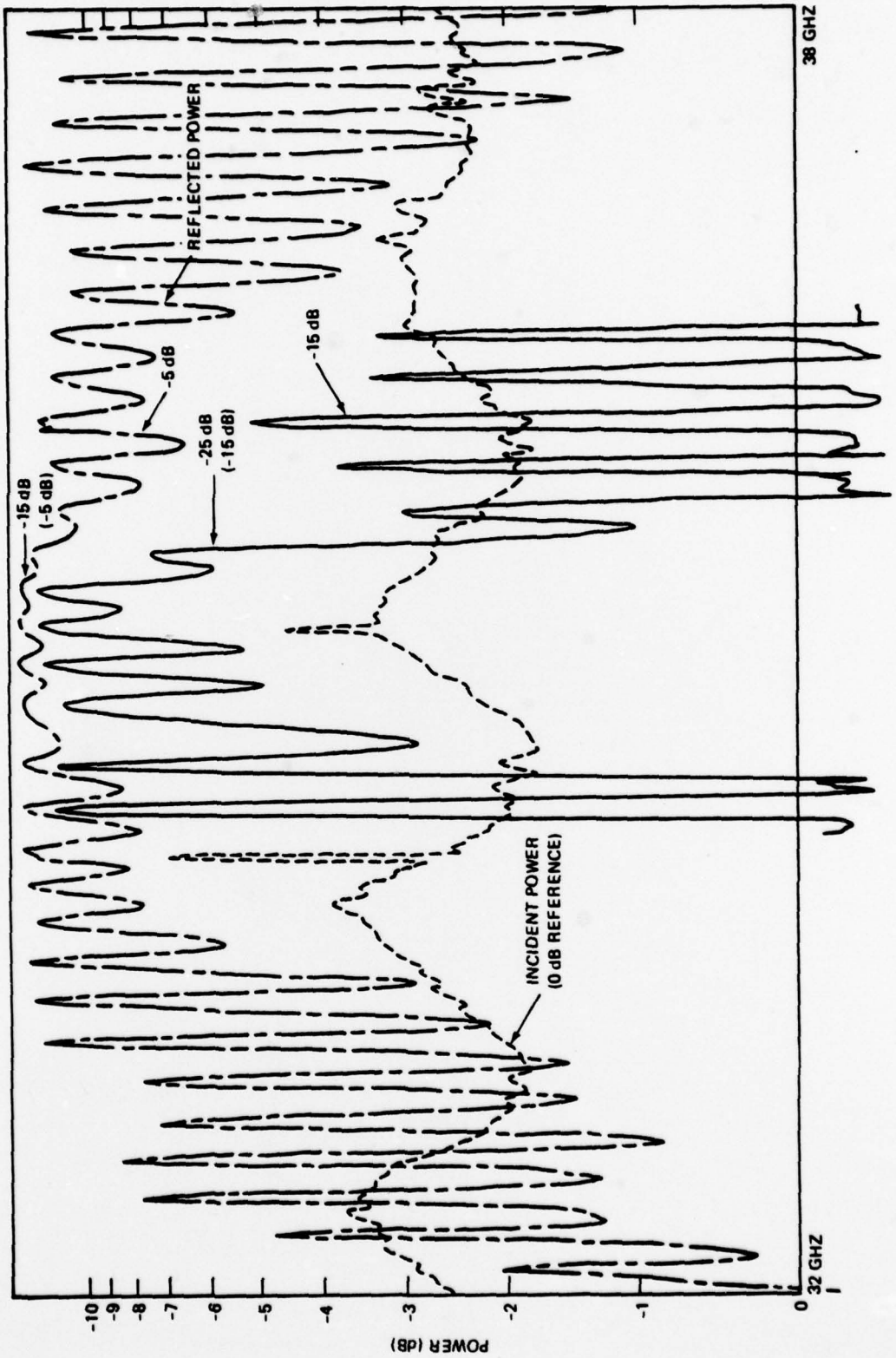

Figure 2.15. Plot of incident and reflected power versus frequency for the large window. The window was mounted in a horn for the test.

Converter and Filter

The gyrotron discussed in this report was designed to produce radiation in the TE_{01}(circular) mode. This mode, while being very low loss, cannot be focused and is difficult to handle. It is therefore desirable to convert the radiation into a rectangular mode, (TE_{10}), which can be focused and can be handled using readily available components. Two converters were commercially available for this purpose. Their specifications are given in Table 2.3. Their reflection and transmission coefficients were measured, and found to be within these specifications. The Hitachi converter seems most likely to with stand high peak powers, and was used in the gyrotron tests. A mode filter, which absorbs all but TE_{on} (circular) modes was used to reduce reflections of non TE_{on} modes, if present.

TABLE 2.3

Converter	Max VSWR	Max Conversion Loss
Hitachi	1.15	0.5 db
TRG	1.10	0.3 db

Detectors-Peak Power

Standard IN53 type broad band crystal detectors were used for measurement of peak powers. These units were individually calibrated using a low level CW signal and thermally compensated Hewlett-Packard thermistor detector. It should be noted that the crystal detectors were used in conjunction with a rectangular waveguide, and thus measured only radiation originally in the TE_{01} (circular) mode.

Detectors-Average Power

A water calorimeter was constructed for measurement of the average gyrotron power. This device is shown in Figure 2.16. Of particular importance is the

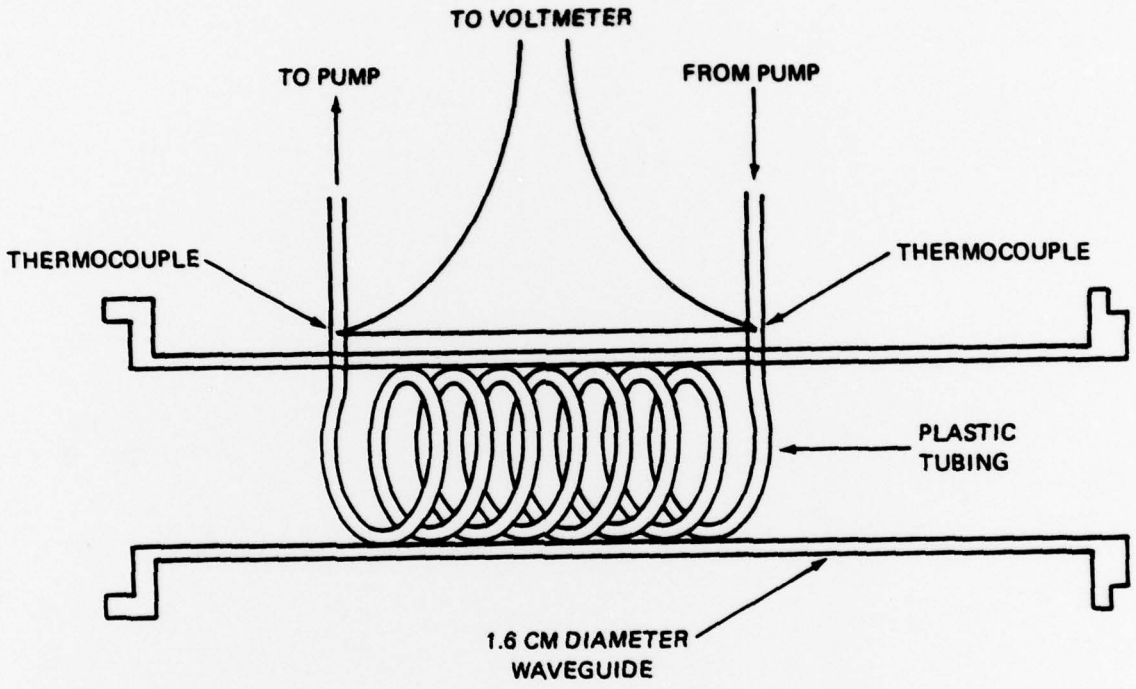

Figure 2.16. Schematic of the calorimeter

fact that the calorimeter is designed to absorb power in all modes. It can thus be used with one of the TE_{on} filters, to determine (by subtraction) the power in non-azimuthally symmetric modes.

The calorimeter consists of six turns of plastic tubing in a 1.60 cm diameter waveguide. Water was pumped through the tubing. A pair of thermocouples was used to measure the change in the water temperature as it passed through the tubing. The device was calibrated using a 20 kw magnetron, pulsed at $\approx$ 100 pps, and a themistor detector. The calorimeter appeared to be accurate to approximately $\pm$ 5%. Care had to be taken to assure that the water flow was the same each time the calorimeter was used in order to achieve this accuracy.

Test Results

Cold Tests

Cold tests (i.e., microwave measurements in the absence of the electron beam) were performed on the cavity and output structure.

The resonant frequency, Q, and field distribution were measured for the two tapered cavities. The apparatus used for this measurement is shown in Figure 2.17. Power was coupled into and out of the cavity via small (2 mm diameter) holes on opposite sides of the cavity, near the mid-point of the cavity. K_a band waveguides were oriented to couple to the H_z of the cavity. The resonant frequency was measured using a standard absorbtion type wavemeter. The Q was determined by measuring 3 db points of the resonance curve.

The field distribution in the cavity was determined by the perturbation method. In this case a .025 cm thick disk of plastic, with a diameter almost as large as that of the cavity was used as the perturbation. The local

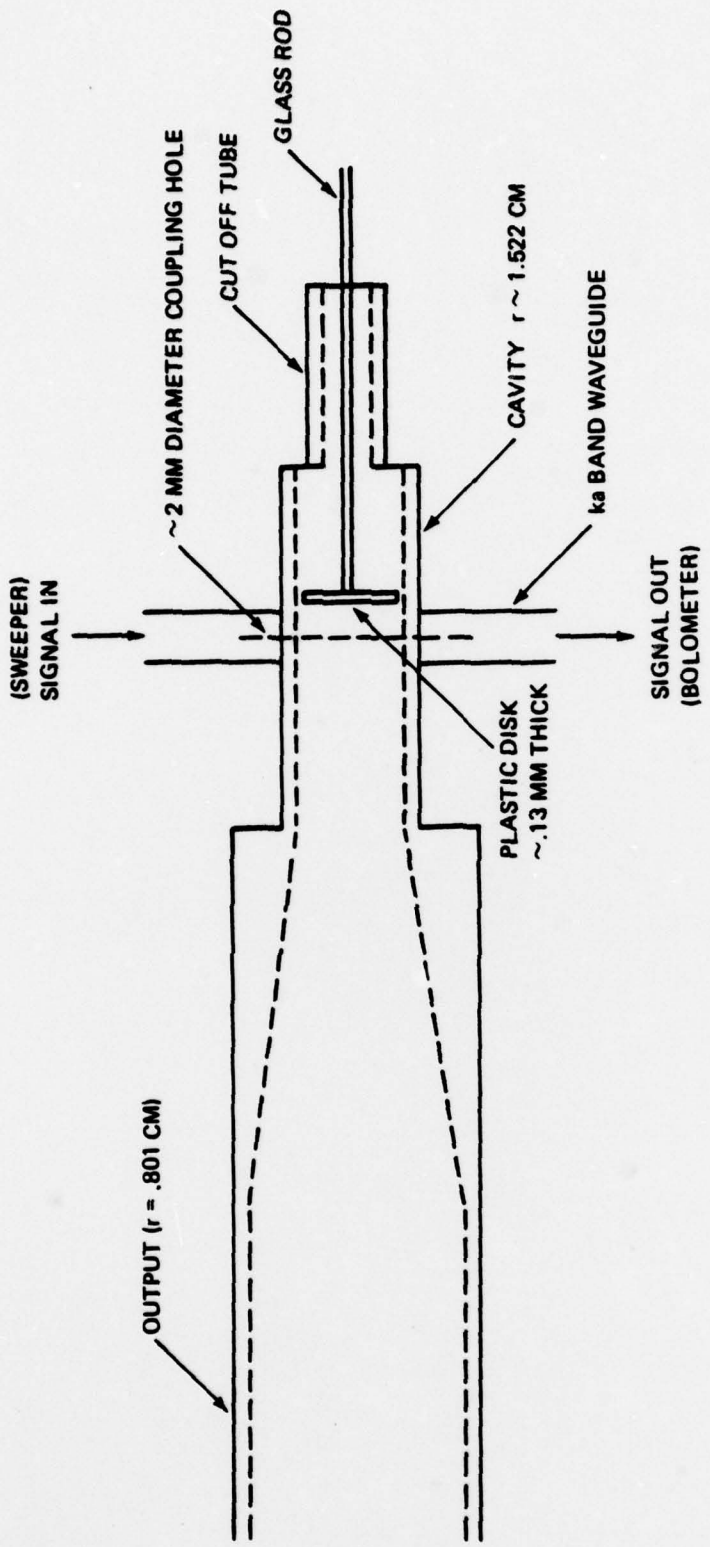

Figure 2.17. Arrangement for test of the cavity parameters

electric field magnitude is inferred from the change in the resonant frequency due to the presence of the disk. The relation is[7]

$$\frac{\delta f}{f_0} = -\frac{\varepsilon_1 - \varepsilon_0}{2\varepsilon_0} \quad \frac{\int_{v_1} E_0^2 dv}{\int_{v_0} E_0^2 dv}$$

where f_0 is the resonant frequency without the disk, Δf is the shift in frequency from f_0, ε_1 and ε_0 are the disk and vacuum permitivities, and v_1 and v_0 are the volumes of the disk and cavity respectively.

The cavity specifications are given in Table 2.4, and the field distribution for cavity #4 in Figure 2.18. The resonant frequencies are approximately as expected. The Q's observed are not as predicted, as it is expected that the longer cavity should have the higher Q. (The longer cavity should have a Q of approximately twice that of the shorter.) In addition, the Q's observed are all above that which are predicted by 2.13. This brings to question either the rather simplified means of calculating Q, and/or the measurement. Both of these possibilities will be pursued, and be reported on in the reports for project 6085. For the purposes of the initial experiment, however, the cold test values will be used.

We note that the field profile for the tapered cavity is weighted toward the output of the cavity; as was expected.

TABLE 2.4

	Cavity #4	Cavity #5
Resonant Frequency (GHz)	35.06	34.975
Q (with 1.143 cm diameter step)	308	330
(with 1.245 cm diameter step)	-	390

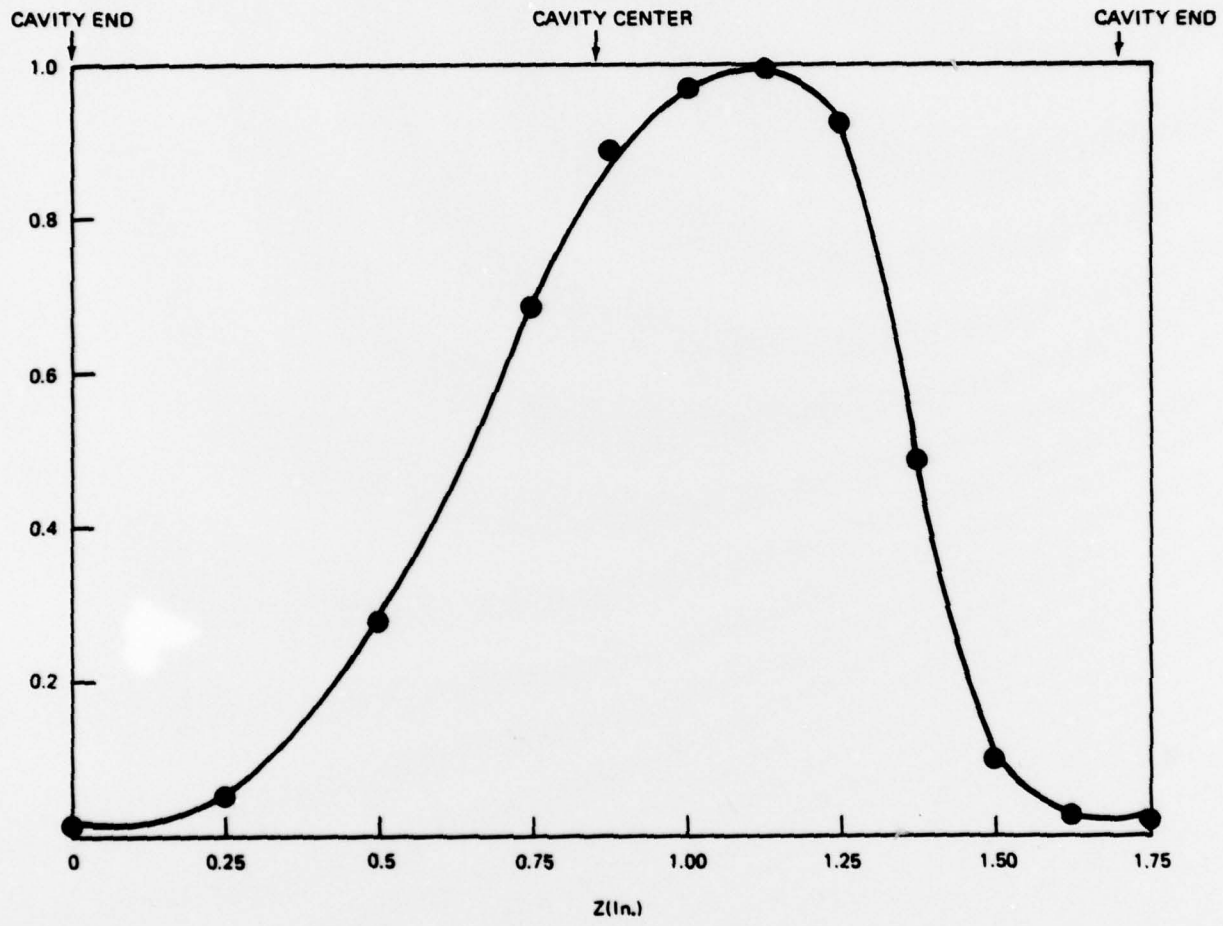

Figure 2.18. Axial electric field profile of cavity #4

Tests with the Electron Beam Present

Preliminary "hot" tests were conducted under this contract. Due to the fact that all of the parts of the system, as well as those of the test facility, were untried, most of this testing was directed toward "debugging." However, the system and test facility are working well, and a full characterization and optimization should be fairly straight forward. These results will be included in the reports for JAYCOR Project #6085.

The general behavior of the device is as follows:

The device oscillated stably, and once the correct parameter regime was determined, with very little adjustment. Repeatability from run to run was excellent, demonstrating the better than one percent stabilities of the power supply, modulator, and magnet controller. Under optimized conditions, the output pulse was quite flat and, within the admittedly poor resolution ($\sim$ 10 MHz) of the cavity wavemeter, fairly monochromatic. A better measurement of the spectrum was attempted using a spectrum analyzer, but the results obtained were inconclusive, probably due to instrumentation difficulties.

The two cavities that are shown in Figure 2.12 were tried. The data obtained with each was not complete enought to determine if the difference in lengths is significant. A cavity with no taper, but with a length the same as the shorter tapered cavity was fabricated, but not tried.

The maximum power obtained was 87 kw; with an efficiency of 12%. The maximum efficiency obtained was 13%, at 77 kw. The pulse length was approximately 1.5 μsec, and the repetition rate $\leq$ 10 pps. The frequency of oscillation was 35.05 GHz, with a tunability of approximately $\pm$ 150 MHz.

The efficiencies and output powers are clearly disappointing. However, measurements made on a long pulse version of the oscillator indicate that

up to 40 percent of the electron beam is being intercepted at the input guide. This will clearly alter the true efficiency, and raises serious questions as to the actual beam size, position, and quality, since by design the beam should have little difficulty passing through the input guide. At the writing of this report, tests are in progress to determine the exact nature of the problem. The results of these tests, and those of measurements made with knowledge of the beam current will be detailed in subsequent reports.

Conclusion

Under contract No. N00173-77-C-0215, JAYCOR has developed methods for the design of gyromonotrons with right circular cavities. Using these methods, a gyromonotron has been designed to operate at 35 GHz with an output power of 170 kw with an efficiency of 30%. This efficiency is in rough agreement with those predicted by others[2,3], for similar devices.

The gyrotron has been fabricated and a gyrotron test facility designed and constructed. The device has undergone initial tests. The results of these tests have indicated much lower efficiencies than predicted, but are most likely complicated by the interception of the beam prior to entry into the cavity. It is believed that this problem can be corrected fairly easily, and complete results of subsequent tests will be reported under JAYCOR Project #6085.

APPENDIX A

MASER TESTING FACILITY

A maser test facility has been established and tested at the NRL site. The basic system consists of: (a) a 5 Mw lumped-line modulator and pulse transformer combination, which has been loaded and tapped to give 70 kv@ 0-15A and 35 kv $\pm$ 3500 v @ 1A with a fixed pulse length of approximately 2 μs, (b) a 40 kg superconducting magnet. The magnet specifications are on file in room 104 of building 51 at NRL, and the approximate field profile is given in Figure 2.11, (c) auxiliary subsystems, including timing circuits, a heater current source and diagnostics, etc. These items are conventional, and their circuit schematics are on file in room 104 of building 51 of the Naval Research Laboratory.

The facility is presently fully operational. It is a straightforward system which has required little maintenance, and should provide good continued service.

Manuals for the individual components of the sytem are located with those instruments, in room 104 of building 51 at the Naval Research Laboratory.

REFERENCES

1. P. Sprangle and A. T. Drobot. "The Linear and Self-Consistent Nonlinear Theory of the Electron Cyclotron Maser Instability"; IEE Trans. MTT-25, 528-544 (1977).

2. K. R. Chu. "Theory of Electron Cyclotron Maser Interactions in a Cavity at the Harmonic Frequencies", NRL Memo Report 3672, (1977).

3. V. A. Flyagin, A. V. Gaponov, M. I. Pelelin, and V. K. Yulpatov. "The Gyrotron", IEE MTT, 25, 1977.

4. S. A. Schelkunoff. Electromagnetic Waves, Van Nostrand Co (NY), 1943.

5. J. L. Seftor, K. R. Chu, and A. T. Drobot. "An Investigation of a Magnetron Injection Gun Suitable for Use in Cyclotron Resonance Masers", NRL Memo Report 3697, (1978).

6. Varian Associate, "Technical Report on the Design of an Electron Gun for a Cyclotron Resonance Maser", under NRL Contract N00173-77-C-0086. (June 1967).

7. M. A. Heald and C. B. Wharton, Plasma Diagnostics with Microwaves, John Wiley and Sons, New York, 1965.